University of Groningen

GATA4 controls regionalization of tissue immunity and commensal-driven immunopathology

Earley, Zachary M.; Lisicka, Wioletta; Sifakis, Joseph J.; Aguirre-Gamboa, Raúl; Kowalczyk, Anita; Barlow, Jacob T.; Shaw, Dustin G.; Discepolo, Valentina; Tan, Ineke L.; Gona, Saideep

Published in:
Immunity

DOI:
10.1016/j.immuni.2022.12.009

IMPORTANT NOTE: You are advised to consult the publisher's version (publisher's PDF) if you wish to cite from it. Please check the document version below.

Document Version
Publisher's PDF, also known as Version of record

Publication date:
2023

Link to publication in University of Groningen/UMCG research database

Citation for published version (APA):
Earley, Z. M., Lisicka, W., Sifakis, J. J., Aguirre-Gamboa, R., Kowalczyk, A., Barlow, J. T., Shaw, D. G., Discepolo, V., Tan, I. L., Gona, S., Ernest, J. D., Matzinger, P., Barreiro, L. B., Morgun, A., Bendelac, A., Ismagilov, R. F., Shulzhenko, N., Riesenfeld, S. J., & Jabri, B. (2023). GATA4 controls regionalization of tissue immunity and commensal-driven immunopathology. *Immunity*, *56*(1), 43-57.e10. https://doi.org/10.1016/j.immuni.2022.12.009

Copyright
Other than for strictly personal use, it is not permitted to download or to forward/distribute the text or part of it without the consent of the author(s) and/or copyright holder(s), unless the work is under an open content license (like Creative Commons).

The publication may also be distributed here under the terms of Article 25fa of the Dutch Copyright Act, indicated by the “Taverne” license. More information can be found on the University of Groningen website: https://www.rug.nl/library/open-access/self-archiving-pure/taverne-amendment.

Take-down policy
If you believe that this document breaches copyright please contact us providing details, and we will remove access to the work immediately and investigate your claim.

Downloaded from the University of Groningen/UMCG research database (Pure): http://www.rug.nl/research/portal. For technical reasons the number of authors shown on this cover page is limited to 10 maximum.

Download date: 31-10-2023

Article

Immunity

GATA4 controls regionalization of tissue immunity and commensal-driven immunopathology

Graphical abstract

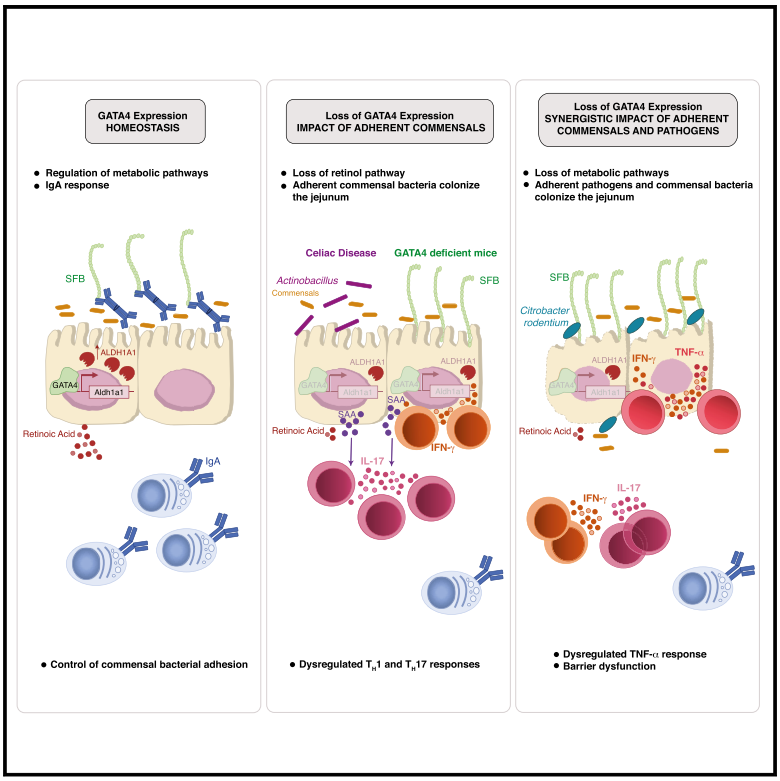

Highlights

- GATA4 prevents small intestinal inflammation by restricting bacterial colonization
- GATA4 regulates bacterial colonization in part by regulating IgA and retinol metabolism
- GATA4 deficiency, SFB, and *Citrobacter rodentium* synergize to drive immunopathology
- Th17 immunity is found in celiac patients with GATA4 deficiency and *Actinobacillus*

Authors

Zachary M. Earley, Wioletta Lisicka, Joseph J. Sifakis, ..., Natalia Shulzhenko, Samantha J. Riesenfeld, Bana Jabri

Correspondence

sriesenfeld@uchicago.edu (S.J.R.), bjabri@bsd.uchicago.edu (B.J.)

In brief

Regulators of intestinal regionalization are vital, yet poorly understood. Here, Earley et al. demonstrate how the transcription factor GATA4 regulates metabolic pathways and luminal IgA to control adherent bacteria colonization. Proper gut regionalization and commensal colonization is critical in preventing dysregulated Th17 responses and immunopathology in humans and mice.

Earley et al., 2023, Immunity *56*, 43–57
January 10, 2023 © 2022 Elsevier Inc.
https://doi.org/10.1016/j.immuni.2022.12.009

CellPress

Immunity

CellPress

Article

GATA4 controls regionalization of tissue immunity and commensal-driven immunopathology

Zachary M. Earley,[1,2] Wioletta Lisicka,[1,2] Joseph J. Sifakis,[3] Raúl Aguirre-Gamboa,[2] Anita Kowalczyk,[2] Jacob T. Barlow,[4] Dustin G. Shaw,[1,2] Valentina Discepolo,[5] Ineke L. Tan,[6] Saideep Gona,[7] Jordan D. Ernest,[2] Polly Matzinger,[8] Luis B. Barreiro,[1,2,7] Andrey Morgun,[9] Albert Bendelac,[1,10] Rustem F. Ismagilov,[4,11] Natalia Shulzhenko,[12] Samantha J. Riesenfeld,[1,2,13,14,*] and Bana Jabri[1,2,10,15,16,*]

[1]Committee on Immunology, University of Chicago, Chicago, IL, USA
[2]Department of Medicine, University of Chicago, Chicago, IL, USA
[3]Department of Chemistry, University of Chicago, Chicago, IL, USA
[4]Division of Biology and Biological Engineering, California Institute of Technology, Pasadena, CA, USA
[5]Department of Medical Translational Sciences and European Laboratory for the Investigation of Food Induced Diseases, University of Federico II, Naples, Italy
[6]Department of Gastroenterology and Hepatology, University of Groningen and University of Medical Center Groningen, Groningen, the Netherlands
[7]Genetics, Genomics, and Systems Biology, University of Chicago, Chicago, IL, USA
[8]Ghost Lab, National Institute of Allergy and Infectious Diseases, National Institutes of Health, Bethesda, MD, USA
[9]College of Pharmacy, Oregon State University, Corvallis, OR, USA
[10]Department of Pathology, University of Chicago, Chicago, IL, USA
[11]Division of Chemistry and Chemical Engineering, California Institute of Technology, Pasadena, CA, USA
[12]Department of Biomedical Sciences, Oregon State University, Corvallis, OR, USA
[13]Pritzker School of Molecular Engineering, University of Chicago, Chicago, IL, USA
[14]Institute for Biophysical Dynamics, University of Chicago, Chicago, IL, USA
[15]Department of Pediatrics, University of Chicago, Chicago, IL, USA
[16]Lead contact
*Correspondence: sriesenfeld@uchicago.edu (S.J.R.), bjabri@bsd.uchicago.edu (B.J.)
https://doi.org/10.1016/j.immuni.2022.12.009

SUMMARY

There is growing recognition that regionalization of bacterial colonization and immunity along the intestinal tract has an important role in health and disease. Yet, the mechanisms underlying intestinal regionalization and its dysregulation in disease are not well understood. This study found that regional epithelial expression of the transcription factor GATA4 controls bacterial colonization and inflammatory tissue immunity in the proximal small intestine by regulating retinol metabolism and luminal IgA. Furthermore, in mice without jejunal GATA4 expression, the commensal segmented filamentous bacteria promoted pathogenic inflammatory immune responses that disrupted barrier function and increased mortality upon *Citrobacter rodentium* infection. In celiac disease patients, low GATA4 expression was associated with metabolic alterations, mucosal *Actinobacillus,* and increased IL-17 immunity. Taken together, these results reveal broad impacts of GATA4-regulated intestinal regionalization on bacterial colonization and tissue immunity, highlighting an elaborate interdependence of intestinal metabolism, immunity, and microbiota in homeostasis and disease.

INTRODUCTION

Each region of the gastrointestinal tract performs distinct physiological functions, with the proximal small intestine optimized to digest and absorb critical nutrients, the distal small intestine to reabsorb bile acids and vitamin B12, and the colon to absorb water and electrolytes.[1] There is growing recognition that bacterial colonization[2] and immune phenotypes[3] are also spatially distributed along the gastrointestinal tract. Yet, little is known about the pathophysiological implications of this regionalization, or the molecular mechanisms regulating it. A key challenge in addressing these questions has been a lack of *in vivo* models that allow changes to the tissue environment in one specific intestinal compartment. Previous studies have shown that in the gut, expression of the transcription factor GATA4 is restricted to duodenal and jejunal intestinal epithelial cells (IECs), and that, in its absence, jejunal IECs acquire an ileum-like transcriptional program.[4,5] However, these studies did not address key questions motivating our study, namely, whether and how a jejunal shift to ileal identity impacts bacterial colonization, tissue immunity, or host susceptibility to pathology.

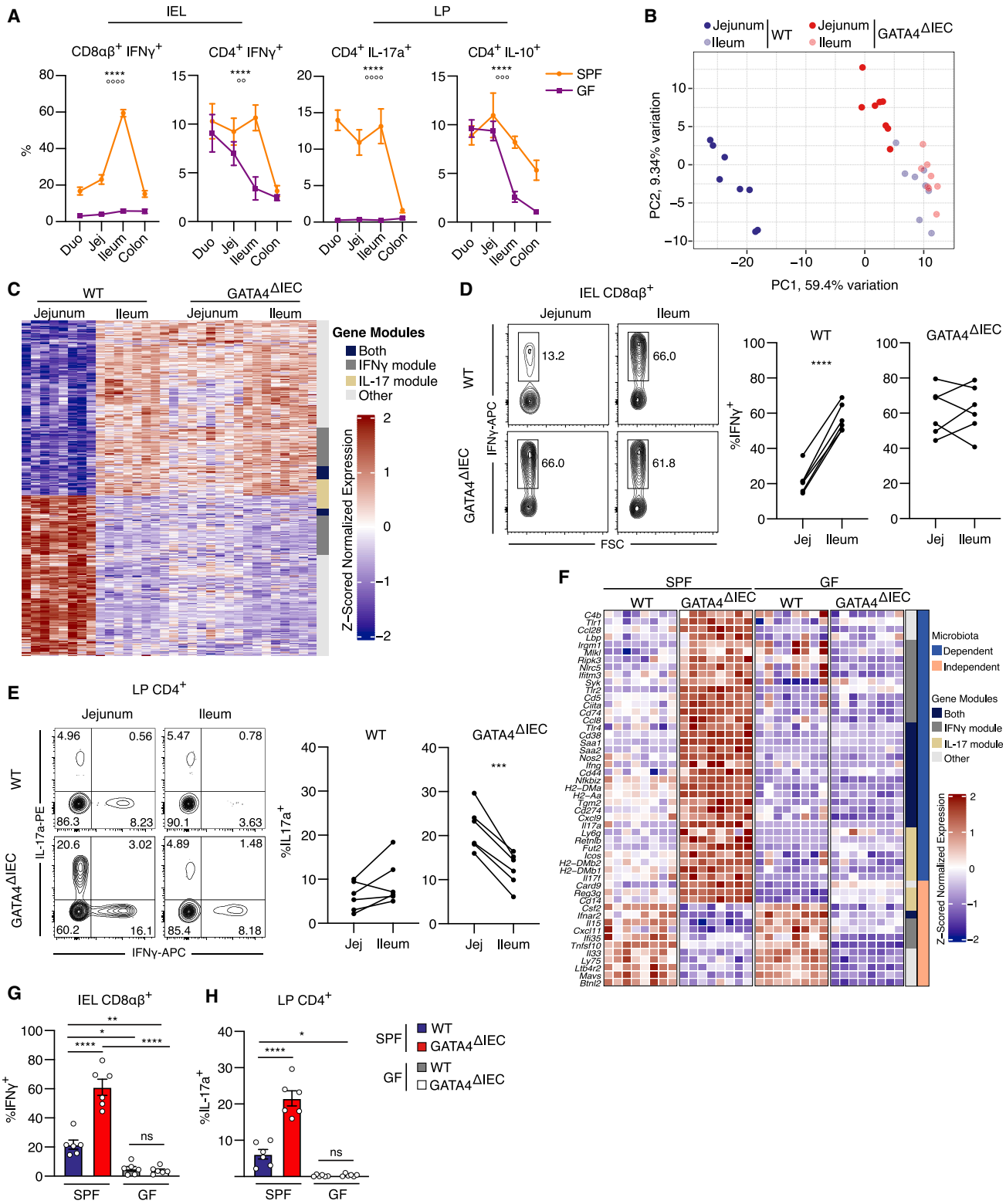

Figure 1. Epithelial GATA4 controls regionalization of tissue immunity in the proximal small intestine

(A) Percentage of IFN-γ+, IL-17a+, or IL-10+ cells among CD4+ or CD8αβ+ T cells from intraepithelial lymphocytes (IELs) or the lamina propria (LP) of each intestinal segment in specific-pathogen-free (SPF) or germ-free (GF) mice. ****p < 0.0001, effect due to region; °°°°p < 0.0001, °°°p < 0.001, °°p < 0.01, effect due to microbiota; two-way ANOVA of microbiota and region impact on cytokine levels. n = 5–7 mice/group.

(legend continued on next page)

RESULTS

GATA4 controls regionalization of intestinal metabolism and immunity

To assess region-specific immune regulation, we analyzed cytokine production in T cells from the intestinal tract of specific-pathogen-free (SPF) and germ-free (GF) mice (Figure 1A). The data revealed that the ileum is uniquely permissive for microbiota-dependent development of inflammatory T cell responses (Figure 1A). To investigate whether GATA4 plays a role in the regionalization of inflammatory immune responses, we performed total jejunal and ileal tissue RNA sequencing (RNA-seq) in GATA4$^{\Delta IEC}$ (*Vil1*$^{cre+}$*Gata4*$^{fl/fl}$) and littermate control wild-type (WT, *Gata4*$^{fl/fl}$) mice. We first confirmed that GATA4 was expressed in duodenal and jejunal, but not ileal or colonic, IECs (Figure S1A). In addition, as previously shown,[5] in the absence of GATA4, jejunal IECs acquired an ileum-like transcriptional program (Figure S1B; Table S1). In particular, GATA4 strongly repressed ileal genes (*Fabp6*, *Slc10a2*) involved in the enterohepatic circulation of bile acids and induced jejunal expression of lipid metabolic genes involved in retinol metabolism (*Adh1*), fat digestion and absorption (*Cd36*, *Fabp1*, *Dgat2*, *Apoa4*), and uptake of vitamins and folate (*Slc46a1*, *Pdxk*) (Figure S1C; Table S1). By comparing the transcriptional profiles of WT jejunum with both WT ileum and GATA4$^{\Delta IEC}$ jejunum, we identified 2,964 GATA4-regulated region-specific genes.

To hone in on immune impacts, we analyzed the 21% (625) of GATA4-regulated region-specific genes that were among 4,279 immune genes we curated from public databases[6,7] (Table S1). The results revealed distinct immune signatures of WT jejunum and ileum, a regionalization of tissue immunity that was lost in GATA4$^{\Delta IEC}$ mice (Figure 1B). Among the immune genes thus identified, more than a third (238) were potential targets of IFN-γ or IL-17 regulation (Figure 1C; Table S2). Consistent with GATA4-regulated regionalization of IFN-γ and IL-17 immune pathways, in the absence of epithelial GATA4, the frequency of intraepithelial IFN-γ$^+$CD8αβ$^+$ T cells in the jejunum increased to the levels observed in the ileum (Figure 1D). Furthermore, GATA4 deficiency led to a heightened Th17 response in the jejunum, with frequencies of IL-17$^+$CD4$^+$ T cells surpassing those in the ileum (Figure 1E). The high levels of IL-17 may be related to additional changes imparted by GATA4 downregulation, such as an increase in serum amyloid A expression (Figure 1F), which is known to amplify Th17 responses in the gut .[8] To determine whether GATA4 was sufficient to induce the jejunal immune signature, we compared previously obtained transcriptional data of ileal epithelial scrapings from either WT or *Rosa26*^{LsL} *Gata4 Vil1*^{cre} (GATA4TG) mice, which selectively overexpress GATA4 in IECs.[9] We observed that the ileum of GATA4TG mice expressed characteristic jejunal immune genes (*Il15ra*, *B2m*) and repressed ileal immune genes (*Saa1/2*, *Nlrc5*, *Cxcr5*) (Figure S1D), indicating that GATA4 is both necessary and sufficient for controlling compartmentalization of immune responses in the small intestine.

We next asked whether the increased IFN-γ and IL-17 T cell responses in the jejunum of GATA4$^{\Delta IEC}$ mice were microbiota dependent. Analyzing the expression of region-specific GATA4-regulated immune genes in the jejunum of GF GATA4$^{\Delta IEC}$ mice revealed that the microbiota were required to drive the elevated IFN-γ- and IL-17-associated genes and T cell responses seen in SPF mice (Figures 1F–1H, S1E, and S1F; Table S1). While a few immune genes, such as *Csf2* (GM-CSF), anti-viral response genes *Ifnar2* and *Mavs*, and the tissue alarmins *Il33* and *Il15*, were GATA4 regulated in a microbiota-independent manner (Figure 1F), most of the microbiota-independent genes were involved in lipid and cholesterol metabolism (Figures S1G and S1H). Furthermore, microbiota-independent genes were more enriched, compared to the microbiota-dependent subset, in direct targets of GATA4 (Figure S1H, Table S1), as indicated by GATA4 binding of promoter regions in published ChIP-seq data (hypergeometric test; $p < 10^{-7}$) (Figure S1H).[10]

Taken together, these results suggest that GATA4 is necessary and sufficient for regulating regional tissue immunity between the proximal and distal small intestine, both by directly controlling the transcription of immune genes in IECs and by blocking the development of microbiota-dependent inflammatory T cell responses in the jejunum.

GATA4 prevents adherent bacteria from colonizing the jejunum

To investigate which microbiota trigger inflammatory immune -responses in the absence of GATA4 in the proximal small intestine, we performed 16S rRNA sequencing of luminal- and mucosal-associated bacterial communities in the jejunum and ileum. This analysis revealed a striking expansion of segmented filamentous bacteria (SFB, *Candidatus arthromitus*) to WT ileum levels in the GATA4$^{\Delta IEC}$ jejunum (Figures 2A, 2B, and S2A), where SFB adhered to IECs (Figure 2C). In WT mice, SFB colonize only the ileum, where they adhere to epithelial cells and induce an antigen-specific Th17 response.[11,12] Consistent with the lack of GATA4 expression in the WT ileum, GATA4$^{\Delta IEC}$ mice demonstrated no changes in ileal bacterial composition (Figure S2A).

(B) Tissue samples plotted by the top two principal components (PCs) of the expression of the 500 most variable immune genes as measured by RNA-seq. n = 8 mice/group.

(C) Heatmap of the z-scored expression of region-specific, GATA4-regulated immune genes (rows) in jejunum and ileum tissue samples (columns) of wild-type (WT) and GATA4$^{\Delta IEC}$ mice. Of 625 genes, 145 are uniquely in the IFN-γ module, 54 are uniquely in the IL-17 module, 39 are in both modules, and 387 are in neither (annotation column). n = 8 mice/group.

(D) Representative (left) and summary (right) plots of the frequencies of IFN-γ$^+$ cells among CD8αβ$^+$ T cells in the IELs. n = 6 mice/group.

(E) Representative (left) and summary (right) plots of the frequencies of IL-17a$^+$ cells among CD4$^+$ T cells in the LP. n = 6 mice/group.

(F) Heatmap of the z-scored expression of 50 selected microbiota-dependent and -independent (right annotation column), region-specific, GATA4-regulated immune genes in jejunum tissue samples from SPF and GF WT and GATA4$^{\Delta IEC}$ mice. Gene modules (left annotation column) as in (C).

(G and H) Frequency (y axis) of IFN-γ$^+$ cells among CD8αβ$^+$ T cells from the IEL (G) or of IL-17a$^+$ cells among CD4$^+$ T cells from the LP (H) in the jejunum of SPF and GF WT and GATA4$^{\Delta IEC}$ mice. n = 6 mice/group.

All data in this figure are pooled from at least two independent experiments. ****$p < 0.0001$, ***$p < 0.001$, **$p < 0.01$, *$p < 0.05$, paired t test (D and E), ANOVA with Tukey multiple comparison test (G and H).

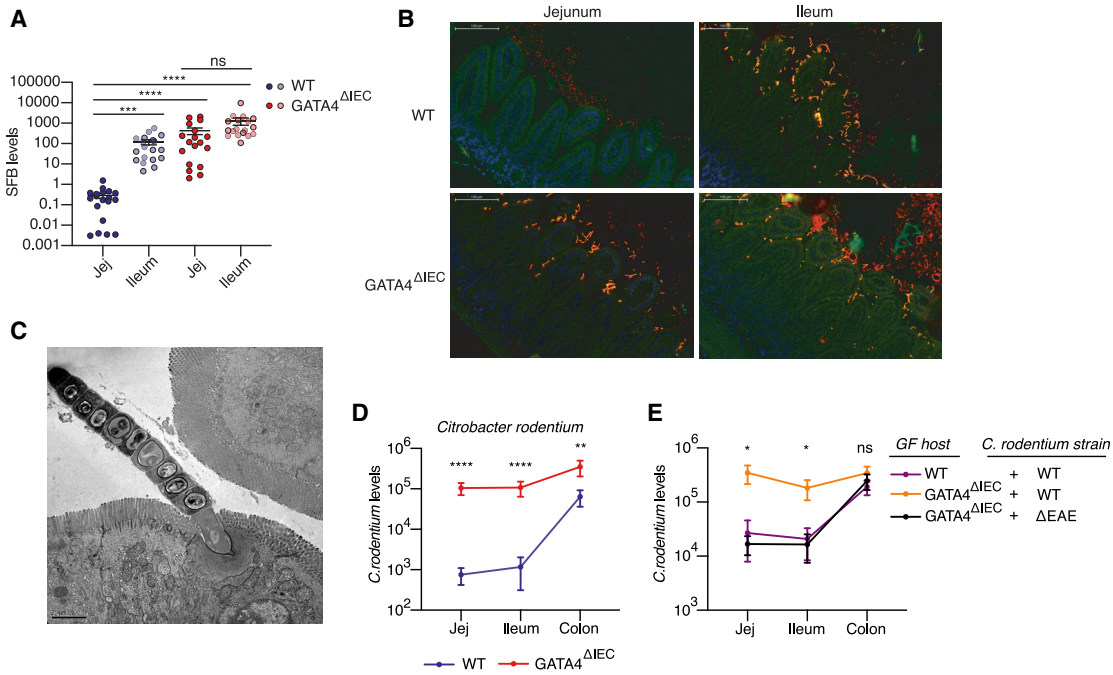

Figure 2. GATA4 prevents commensal and pathogenic bacteria from colonizing the jejunum

(A) SFB load, as measured by qPCR, relative to the amount of host DNA in mucosal scrapings of jejunum and ileum from WT and GATA4$^{\Delta IEC}$ mice. n = 18–19 mice/group.

(B) *FISH* staining using universal 16s rRNA probes (Alexa 546, red-orange), SFB 16s probe (Alexa 488), and counterstained with DAPI (blue). The overlay of the 16s probes (yellow-orange) represents SFB. Figure is a representative image from 4 independent WT and GATA4$^{\Delta IEC}$ mice.

(C) Transmission electron microscopy of SFB adhering to jejunal IECs of GATA4$^{\Delta IEC}$ mice. Figure is a representative image from 3 separate mice and a minimum of 5 different areas of view.

(D) *C. rodentium* load, measured by qPCR relative to host DNA, in distinct intestinal segments in WT and GATA4$^{\Delta IEC}$ mice. n = 13 mice/group.

(E) Bacterial loads of wild-type *C. rodentium* and the ΔEAE mutant, measured by qPCR relative to host DNA, in distinct intestinal segments of GF WT or GATA4$^{\Delta IEC}$ mice. n = 7–9 mice/group.

All data in this figure are pooled from at least two independent experiments and represented as mean ± SEM; ****$p < 0.0001$, ***$p < 0.001$, **$p < 0.01$, *$p < 0.05$, Kruskal-Wallis with Dunn multiple comparison test (A, E), Mann-Whitney test (D).

To assess other commensal bacteria, we transplanted GF mice with altered Schaedler flora (ASF), a defined eight-member bacterial community, which resulted in an expansion of mucus-associated *Mucispirillum schaedleri*[13] in the jejunum of GATA4$^{\Delta IEC}$ but not littermate control WT mice (Figure S2B). These data suggest that epithelial GATA4 expression limits colonization by mucus-resident or adherent bacteria.

To assess whether GATA4 indeed plays such a role, we analyzed the colonization pattern of rat SFB, which cannot adhere to mouse IECs but can stably colonize the lumen of GF mice.[14] In contrast to mouse SFB, rat SFB showed no difference in its capacity to colonize the lumen of WT and GATA4$^{\Delta IEC}$ mice (Figure S2C). The capacity of SFB to adhere may be a critical feature driving its regionalization in a GATA4-dependent manner; however, this cannot be formally demonstrated because rat SFB is only 86% identical to mouse SFB, and other biochemical activities may be involved.[15] We therefore extended our analysis to *Citrobacter rodentium*, an adherent pathogen that preferentially colonizes the colon[16,17] and can be genetically modified. In the absence of GATA4, the niche for *C. rodentium* was altered such that, by seven days after infection, the pathogen colonized the small intestine at levels approaching those in the colon of WT mice (Figure 2D). Using the mutant ΔEAE *C. rodentium,* which lacks the gene intimin required for adherence to IECs, we confirmed that *C. rodentium*'s capacity to colonize the small intestine of GATA4$^{\Delta IEC}$ mice depended on its ability to adhere to IECs (Figure 2E).

Taken together, these results suggest that a key role of GATA4 is to prevent adherent bacteria from interacting with IECs of the proximal small intestine, whose primary function is to ensure the absorption of nutrients. They also suggest that the tissue microenvironment in the jejunum, created through the expression of GATA4, actively prevents colonization of the small intestine by colonic bacteria.

Changes in SFB colonization enhance inflammatory T cell immunity to *C. rodentium*

We next sought to determine whether the presence of SFB adhering to jejunal IECs was required and sufficient for the observed increase in inflammatory host immunity in the jejunum of GATA4$^{\Delta IEC}$ mice (Figures 1B–1E). To evaluate necessity, microbial communities lacking mouse SFB were transplanted into GF GATA4$^{\Delta IEC}$ mice. Specifically, GF GATA4$^{\Delta IEC}$ mice were transplanted with (1) ASF, (2) jejunal microbiota from a WT donor within our colony in which SFB was undetectable, and (3) fecal microbiota from SFB-free C57BL/6J mice from Jackson laboratory (JAX). In all instances, these microbes failed

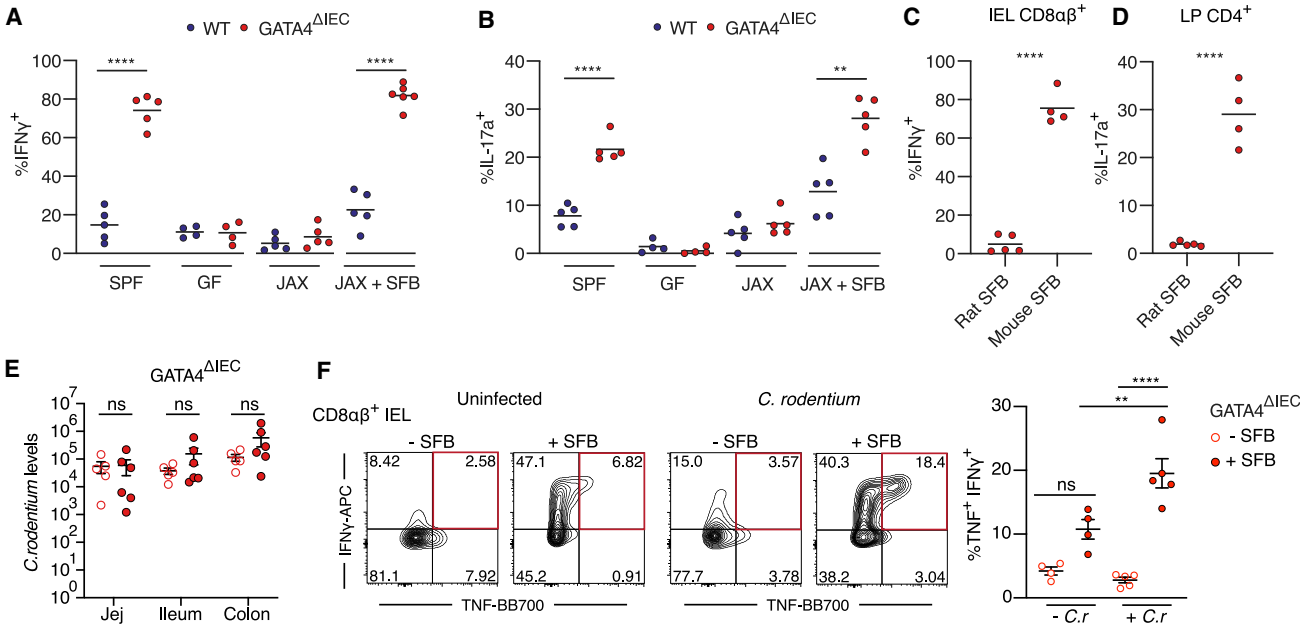

Figure 3. SFB colonization of the proximal small intestine drives excessive inflammatory T cell responses to *C. rodentium* infection

(A and B) Frequency of IFN-γ^+ cells among CD8$\alpha\beta^+$ T cells (A) or IL-17a$^+$ cells among CD4$^+$ T cells (B) in the jejunum from SPF, GF, Jackson (JAX) microbiota transfer, and Jackson microbiota + SFB transfer into GF WT and GATA4$^{\Delta IEC}$ mice. n = 4–6 mice/group.

(C and D) Frequency of IFN-γ^+ cells among CD8$\alpha\beta^+$ T cells (C) and of IL-17$^+$ cells among CD4$^+$ T cells (D) in jejunum of GATA4$^{\Delta IEC}$ mice monocolonized with rat or mouse SFB. n = 5 mice/group.

(E) *C. rodentium* load, measured by qPCR, in distinct intestinal segments in SFB free (open circles) or SFB colonized (filled circles) GATA4$^{\Delta IEC}$ mice. n = 5–6 mice/group.

(F) Representative (left) plots and summarized (right) of IFN-γ^+ and TNF$^+$ CD8$\alpha\beta^+$ IEL T cells from the jejunum of GATA4$^{\Delta IEC}$ mice that are colonized with JAX (open circle) or JAX + SFB (solid circle) and either uninfected (−*C.r*) or infected (+*C.r*) with *C. rodentium*. Red box indicates double IFN-γ^+ TNF$^+$ CD8$\alpha\beta^+$ T cells which are summarized (right). Mice were analyzed 5 days after infection. n = 4–5 mice/group.

All data in this figure are pooled from at least two independent experiments and represented as mean or mean ± SEM; ****$p < 0.0001$, ***$p < 0.001$, **$p < 0.01$, *$p < 0.05$, ns $p > 0.05$, t test (A–D), Mann-Whitney test (E), ANOVA with Tukey multiple comparison test (F).

to induce IFN-γ^+CD8$\alpha\beta^+$ T cells and Th17 cells in the jejunum of GATA4$^{\Delta IEC}$ mice (Figures 3A, 3B, S3A, and S3B). To determine the sufficiency of SFB, we supplemented JAX microbiota or monoassociated GF GATA4$^{\Delta IEC}$ mice with SFB and observed a significant induction of IFN-γ^+CD8$\alpha\beta^+$ T cells and Th17 cells in the jejunum of GATA4$^{\Delta IEC}$ mice to SPF levels (Figures 3A–3D). Furthermore, non-adherent rat SFB was unable to induce appreciable T cell responses in the jejunum of GATA4$^{\Delta IEC}$ mice (Figures 3C and 3D). Finally, to exclude the possibility that another microbe intrinsic to the GATA4$^{\Delta IEC}$ microbiota was driving inflammation, we transplanted GATA4$^{\Delta IEC}$ and littermate control WT microbiota into GF WT and GF GATA4$^{\Delta IEC}$ hosts, respectively. We found that the host genotype determined the immune outcome, irrespective of the input microbial community (Figures S3A and S3B). These data conclusively demonstrate that jejunal colonization of SFB drives the loss of compartmentalization of inflammatory T cell immunity seen in GATA4$^{\Delta IEC}$ mice.

Since SFB colonization induces an antigen-specific Th17 cell response against the 3340 epitope of SFB,[12] we asked whether the increased Th17 cell response observed in the jejunum was a consequence of altered T cell priming. Congenically marked CD45.1$^+$7B8$^+$CD4$^+$ T cells, specific to the 3340 epitope of SFB, differentiated into RORγt$^+$Foxp3$^-$CD4$^+$ T cells selectively in the draining ileal mesenteric lymph nodes (MLNs) of WT mice (Figure S3C), as previously reported.[3] In contrast, in GATA4$^{\Delta IEC}$ mice, RORγt$^+$Foxp3$^-$CD4$^+$ T cells were expanded in the jejunal MLNs, indicating a change in regional T cell priming against SFB (Figure S3C). Furthermore, nine days after transfer, 7B8$^+$ T cells expanded (Figure S3D) and decreased expression of their TCR in the jejunum of GATA4$^{\Delta IEC}$ versus WT mice (Figure S3E). These data indicate that the jejunal bacterial colonization resulting from GATA4 deficiency causes priming of SFB-specific T cells in the jejunal draining lymph nodes, as well as their expansion and activation in the proximal portion of the small intestine.

We next investigated whether altered regionalization of SFB led to dysregulated host immune responses to a competing pathogen in the proximal small intestine. In line with previous studies,[11] the presence of SFB decreased the load of *C. rodentium* in the colon of WT mice (Figure S3F). However, in GATA4$^{\Delta IEC}$ mice, SFB did not decrease the load of *C. rodentium* in either the small intestine or the colon (Figure 3E). Furthermore, the presence of SFB promoted excessive inflammatory immune responses to *C. rodentium* in the jejunum of GATA4$^{\Delta IEC}$ mice (Figures 3F and S3G). Specifically, there was a marked increase in TNF$^+$IFN-γ^+ CD8$\alpha\beta^+$ IEL T cells (Figure 3F) and IFN-γ^+CD4$^+$ T cells from the lamina propria (LP) (Figure S3G) as early as 5 days post infection, a time at which *C. rodentium* did not induce an adaptive immune response in the jejunum in SFB-negative GATA4$^{\Delta IEC}$ mice

(Figures 3F and S3G). In contrast, SFB-dependent homeostatic Th17 and CD8$\alpha\beta^+$IFN-γ^+ responses were not synergistically elevated by *C. rodentium* (Figures S3H and S3I).

Altogether, these results suggest that changes in SFB colonization in the jejunum alter the intestinal immune response to *C. rodentium*, in particular, by driving the expansion of inflammatory TNF$^+$IFN-γ^+CD8$\alpha\beta^+$ T cell immune responses.

Dysregulated immune responses to SFB drive TNF-induced immunopathology after infection

We asked whether the heightened and altered inflammatory immune response to *C. rodentium* infection observed in SFB-colonized GATA4-deficient mice led to increased pathology. GATA4$^{\Delta IEC}$ mice developed severe colitis and villous atrophy in the ileum ten days after infection, symptoms not associated with the infection in WT littermate control mice (Figures 4A and S4A). Furthermore, the intestinal barrier was compromised in GATA4$^{\Delta IEC}$ mice with *C. rodentium* translocating to systemic sites, including the MLNs, liver, and spleen (Figure 4B). By day 12 post-infection, 87.5% of GATA4$^{\Delta IEC}$ mice had died (Figure 4C), punctuating the critical role of GATA4-dependent intestinal regionalization in controlling host disease susceptibility to an enteric pathogen. Consistent with SFB driving dysregulated inflammatory immune responses to *C. rodentium*, albeit without altering *C. rodentium* colonization, the increased mortality observed in GATA4$^{\Delta IEC}$ mice was dependent on the presence of SFB (Figure 4D).

We next pursued how SFB increased the mortality of GATA4$^{\Delta IEC}$ mice infected by *C. rodentium*. TNF and IFN-γ can disrupt intestinal epithelial barrier function.[18–20] We hypothesized that the synergistic effect of SFB and *C. rodentium* on inflammatory TNF and/or IFN-γ immune responses (Figure 3F) disrupted epithelial barrier function and thereby caused bacterial translocation. In accordance with that hypothesis, SFB-colonized GATA4$^{\Delta IEC}$ mice infected with *C. rodentium* had decreased expression of tight junction and barrier proteins (Figure 4E) and increased translocation of *C. rodentium* to the MLNs (Figure 4F), compared to SFB-free, infected GATA4$^{\Delta IEC}$ mice. In line with other studies,[21,22] treatments that neutralize IFN-γ and IL-17a increased mouse mortality (Figure S4B). In contrast, anti-TNF treatment reduced *C. rodentium* translocation (Figure 4G), restored expression of *Tjp2* (Figure S4C), and increased survival (Figure 4H), consistent with a previous finding that TNF-neutralizing antibodies restore barrier function in Crohn's disease patients.[20]

Taken together, these data highlight how, in the context of GATA4 deficiency, SFB promotes *C. rodentium*-induced immunopathology by increasing dysregulated TNF-producing T cell responses. More generally, this observation reveals a previously unknown role of commensal bacteria regionalization in promoting pathogenic versus protective immune responses to pathogens.

GATA4 regulates retinol metabolism and luminal IgA levels to control colonization of SFB

Based on our finding that SFB colonization of the proximal small intestine in GATA4$^{\Delta IEC}$ mice was responsible for the severe immunopathology observed upon *C. rodentium*-infection, we sought to understand how GATA4 restricts SFB colonization of the WT proximal small intestine. A previous report revealed that B cell-deficient mice display lipid metabolic defects in the jejunum, as well as a gene expression signature associated with GATA4$^{\Delta IEC}$ mice.[23] We therefore asked whether B cell-deficient JH mice, which lack the JH gene segments necessary for BCR recombination,[24] recapitulate the bacterial colonization defect observed in GATA4-deficient mice (Figure 2). Monocolonization of GF JH-deficient mice with *C. rodentium* or SFB led to their expansion in the jejunum (Figures S5A–S5C), phenocopying GATA4$^{\Delta IEC}$ mice. Since a substantial proportion of the microbiota, and in particular, SFB, is coated by IgA,[25–27] we asked whether the change in bacterial colonization in B cell-deficient mice was mediated through IgA. In agreement with previous studies,[28] SFB expanded in the ileum of IgA-deficient (*Igha*$^{-/-}$) mice (Figure S5D). More importantly, monocolonization of GF *Igha*$^{-/-}$ mice with SFB led to an expansion in the jejunum to levels equivalent to those found in the ileum of WT mice (Figures 5A and 5B). In contrast, *C. rodentium* was not altered in IgA-deficient mice (Figure S5E). This finding is consistent with *C. rodentium* being coated in the intestinal lumen by IgG and not IgA[29] and suggests that GATA4, through yet unknown mechanisms that may involve changes in the metabolic milieu, prevents *C. rodentium* colonization of the small intestine.

Given these observations, we asked whether GATA4 may control SFB colonization by regulating the regional distribution of IgA$^+$ plasma cells in the small intestine. We found that the jejunum contained approximately three times as many IgA$^+$B220$^-$ plasma cells as the ileum (Figure 5C) and that the higher numbers of IgA-producing plasma cells were associated with a greater capacity to produce IgA in tissue explants (Figure S5F). This regionalization of IgA response was GATA4 dependent, as evidenced by significantly reduced numbers of IgA$^+$B220$^-$ plasma cells (Figure 5C) and IgA production (Figure S5F) in the jejunum of GATA4$^{\Delta IEC}$ versus WT mice. The overall result was a substantial decrease in luminal secretory IgA in the jejunum of GATA4$^{\Delta IEC}$ mice (Figure 5D). Reduced luminal IgA was also observed in the jejunum of GF GATA4$^{\Delta IEC}$ mice, indicating that the reduction is independent of microbiota (Figure S5G). Moreover, free-IgA in the jejunal luminal content from GATA4$^{\Delta IEC}$ mice had less capacity than that of littermate-control WT mice to coat an IgA-unbound microbiota taken from the feces of *Rag1*$^{-/-}$ mice (Figures 5E and S5H). We next tested whether exogenous luminal IgA was sufficient to rescue the luminal IgA defect and prevent colonization of the jejunum by SFB in GATA4$^{\Delta IEC}$ mice. Polyclonal luminal sIgA, capable of strongly coating microbes from *Rag1*$^{-/-}$ feces, were isolated from the intestinal contents of WT mice with protein L magnetic beads (Figure S5I). This luminal polyclonal IgA or PBS (PBS) was gavaged to GF WT or GATA4$^{\Delta IEC}$ mice prior to and after colonization with SFB (Figure S5J). This IgA was indeed sufficient to prevent SFB from colonizing the jejunum of GATA4$^{\Delta IEC}$ mice (Figure 5F). These results indicate that GATA4-dependent regulation of luminal IgA in the proximal small intestine prevents SFB colonization.

Since the IgA defect was microbiota independent, we hypothesized that epithelial GATA4 mediated IgA levels by controlling region-specific metabolic processes. To identify potential candidates, we performed gene set enrichment analysis of the differentially expressed, i.e., GATA4-dependent region-specific, genes in our epithelial RNA-seq data and in published GATA4TG data (Figures S1B and S1D), which revealed retinol

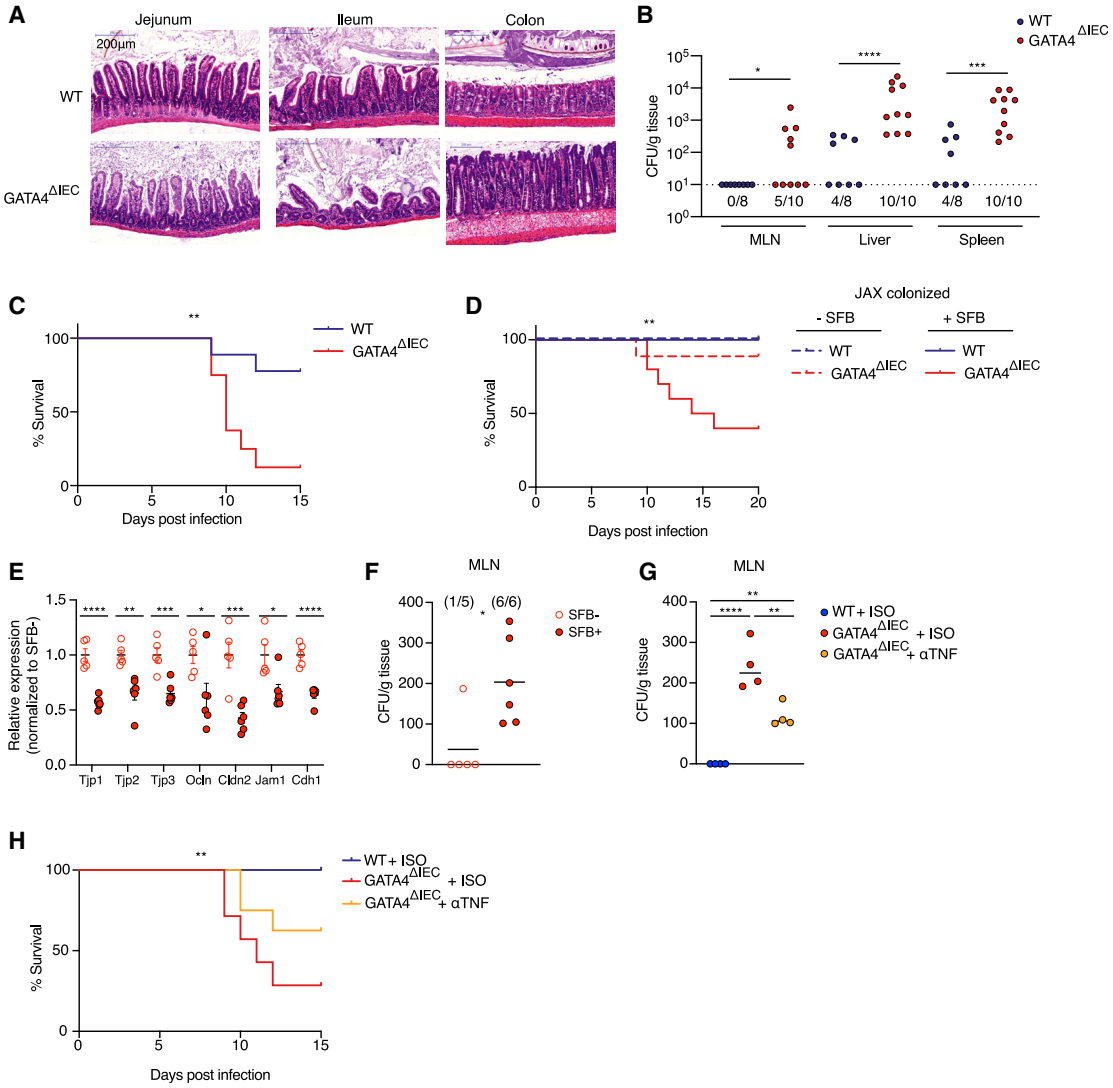

Figure 4. Dysregulated SFB colonization of the proximal intestine promotes loss of barrier function and TNF induced immunopathology upon *C. rodentium* infection

(A) Representative H&E staining of each intestinal region 10 days after *C. rodentium* infection.

(B) CFUs of *C. rodentium* translocation to MLN, liver, and spleen. n = 8–10 mice/group.

(C) Percent survival of WT and GATA4$^{\Delta IEC}$ mice 0–15 days after *C. rodentium* infection. n = 8–9 mice/group.

(D) Percent survival of JAX colonized WT (blue) and GATA4$^{\Delta IEC}$ (red) in SFB-associated (solid lines) or SFB-free mice (dashed lines) 0–20 days after *C. rodentium* infection. n = 6 WT mice/group, n = 9 GATA4$^{\Delta IEC}$ – SFB mice/group, n = 10 GATA4$^{\Delta IEC}$ + SFB mice/group.

(E) Relative expression as measured by qPCR of tight junction proteins to GAPDH in the jejunum of SFB-free (open circles) or SFB-colonized (filled circles) GATA4$^{\Delta IEC}$ mice 5 days after infection. n = 5–6 mice/group.

(F) CFUs of *C. rodentium* translocation to MLN of SFB-free or SFB-colonized GATA4$^{\Delta IEC}$ mice 5 days after infection. n = 5–6 mice/group.

(G) CFUs of *C. rodentium* translocation to MLN of SFB-positive WT isotype, GATA4$^{\Delta IEC}$ isotype, or GATA4$^{\Delta IEC}$ αTNF-treated mice 5 days after infection. n = 4 mice/group.

(H) Percent survival of WT isotype-treated, and GATA4$^{\Delta IEC}$ isotype-treated, or αTNF-treated mice 0–15 days after *C. rodentium* infection. n = 7–9 mice/group. All data in this figure are pooled from at least two independent experiments and represented as mean or mean ± SEM; ****$p < 0.0001$, ***$p < 0.001$, **$p < 0.01$, *$p < 0.05$, Mann-Whitney test (B), Mantel-Cox test (C, D, H), t test (E), Mann-Whitney test (F), ANOVA with Tukey multiple comparison test (G).

metabolism as a top enriched KEGG pathway (Figures S5K and S5L). Genes in the retinol metabolic pathway were elevated in the jejunum of WT mice, relative to ileum-like tissues (Figure 5G), supporting previous reports that the proximal intestine facilitates greater vitamin A uptake and metabolism.[30,31] Conversely, GATA4TG mice induced retinol metabolic genes in the ileum, indicating that GATA4 was both necessary and sufficient to control its regionalization (Figure S5L).

In fact, direct transcriptional regulation of retinol metabolism by GATA4 in IECs was suggested by our analysis of published ChIP-seq data,[9,10] which found an enrichment of GATA4-binding promoters among the differentially expressed, versus not differentially

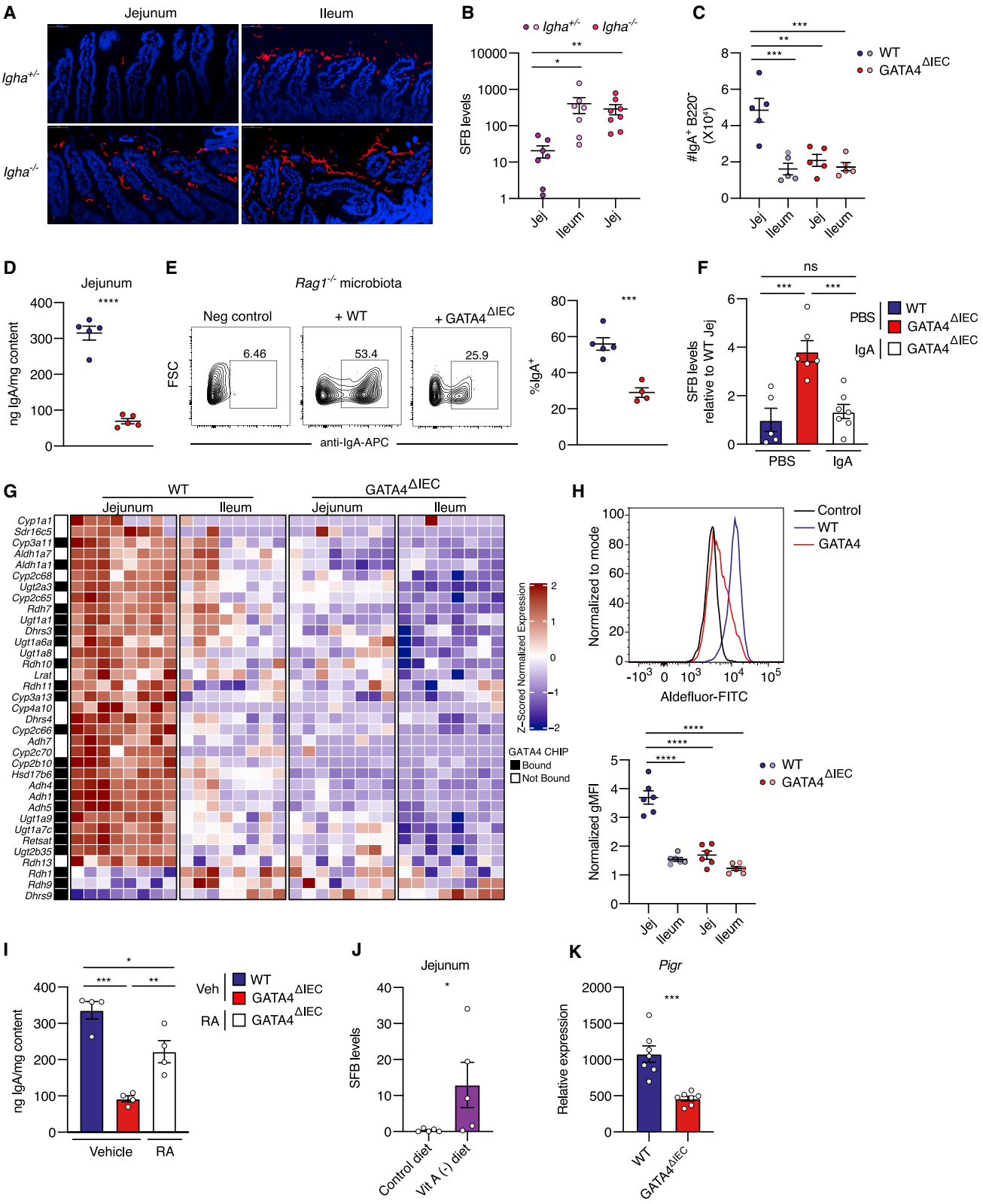

(legend on next page)

expressed, epithelial genes in the retinol metabolism pathway (Figure 5G; Table S1; odds ratio 2.6, $p < 0.005$; Fisher exact test). The rate-limiting enzyme in RA production, *Aldh1a1* (RALDH1), was directly bound by GATA4 in a ChIP-seq study[10] (Figure 5G). Concordantly, in the absence of GATA4, jejunal epithelial cells exhibited impaired aldehyde dehydrogenase (ALDH) activity, indicating a decreased capacity to produce retinoic acid (RA) (Figure 5H). RA regulates intestinal B cell responses, including intestinal homing receptors on B cells (CCR9, $\alpha4\beta7$) and IgA class switching.[32] In addition, epithelial RARα/β regulates the number of IgA-producing B cells.[33,34] To determine whether the defect in luminal IgA in the small intestine of GATA4$^{\Delta IEC}$ mice could be rescued with exogenous RA, we injected GATA4$^{\Delta IEC}$ mice intraperitoneally with RA for two weeks. RA augmented luminal IgA levels in the jejunum of GATA4$^{\Delta IEC}$ but not WT mice (Figures 5I and S5M). Conversely, in mice fed a vitamin A-deficient diet, SFB colonized the jejunum (Figure 5J). Exogenous RA did not fully restore WT levels of IgA and failed to reduce jejunal SFB in GATA4$^{\Delta IEC}$ mice (Figure S5N). This result suggests that GATA4 regulates luminal IgA levels through additional mechanisms. In line with this hypothesis, we observed that GATA4 induces jejunal expression of the polymeric immunoglobulin receptor (PIGR) (Figure 5K), which regulates IgA transcytosis.[35]

Taken together, these data indicate that, by controlling regional retinol metabolism, expression of PIGR, and potentially other aspects of IECs, GATA4 regulates luminal IgA, which in turn restricts SFB colonization of the proximal small intestine.

Loss of GATA4 expression in celiac disease is associated with regional tissue defects and increased IL-17 immunity

Celiac disease (CeD) is an auto-immune-like Th1-mediated enteropathy of the duodenum caused by dietary gluten in genetically susceptible individuals.[36] A long-standing conundrum has been the increase of gluten-dependent, but not gluten-specific, duodenal Th17 responses in CeD patients.[37–39] During active CeD (ACeD), patients exhibit alterations in IECs,[36,40] as well as lipid[41] and vitamin deficiencies.[42] We therefore hypothesized that ACeD patients have decreased expression of *GATA4* in IECs and that this decrease could be associated with reported changes in their microbiota[43,44] and increased IL-17 immunity.

To investigate this possibility, we compared the transcriptional profiles of duodenal biopsies from ACeD patients, CeD patients on a gluten-free diet (GFD), and control patients with non-inflammatory intestinal symptoms that required upper endoscopies.[45] The analysis revealed that a subset of active celiac patients had lower *GATA4* expression, compared to control subjects, which was restored by a GFD (Figure 6A). Immunohistochemistry staining confirmed at the protein level that there are ACeD patients with low and high GATA4 expression (Figure 6B). Furthermore, in ACeD, loss of GATA4 protein production was specifically seen in apical epithelial cells, whereas intestinal crypts cells retained GATA4 production (Figure 6B). Overall GATA4 expression was inversely correlated with severe tissue damage in ACeD, as measured by the APOA4/KI67 ratio[46] (Figure S6A). However, we also observed that GATA4 expression could be preserved in ACeD with severe villous atrophy (Figure 6B). This observation suggests that other factors in addition to GATA4 influence the degree of tissue damage and that IECs lining the damaged mucosa may exhibit distinct transcriptional programs, independently of the severity of villous atrophy.

To gain insight into the impact of low *GATA4* expression in ACeD, we identified genes that were differentially expressed between 42 "GATA4-hi" individuals (18 control, 6 ACeD, and 18 GFD), defined by *GATA4* expression above the 70th percentile of the entire cohort, and 15 "GATA4-lo" ACeD patients, defined by *GATA4* expression below the 30th percentile of ACeD patients (Figure S6B; Table S3). Genes expressed in GATA4-lo patients were enriched, relative to GATA4-hi individuals, in the human orthologs of genes specifically expressed in mouse ileum-like tissues (WT ileum and GATA4$^{\Delta IEC}$ jejunum), versus the jejunum (Figures 6C and S6C). Similarly, GATA4-hi specific genes were enriched in human orthologs of genes specific to the mouse jejunum, relative to ileum-like tissues (Figures 6C and S6C). Thus, during ACeD, intestinal regionalization may be lost as the duodenum decreases expression of GATA4-dependent jejunum-specific genes and increases expression of ileum-specific genes.

Many of the jejunal genes increased in GATA4-hi patients are direct targets of GATA4 and involved in lipid metabolic processes, such as cholesterol absorption and retinol metabolism (Figure 6D). Compared to GATA4-hi individuals, GATA4-lo ACeD patients demonstrated reduction in retinol metabolic genes and increased

Figure 5. GATA4 regulates regionalization of retinol metabolism and IgA to limit SFB colonization in the proximal intestine

(A) FISH staining of SFB (Cy5) in monocolonized IgA-deficient (*Igha*$^{-/-}$) and littermate control (*Igha*$^{+/-}$) mice and counterstained with DAPI.

(B) SFB load, as measured by qPCR, in mucosal scrapings from the jejunum and ileum of control (*Igha*$^{+/-}$) mice and the jejunum of IgA-deficient (*Igha*$^{-/-}$) mice. n = 7–8 mice/group.

(C) Number of IgA^{+}B220^{-} plasma cells, in the jejunum and ileum tissue of WT and GATA4$^{\Delta IEC}$ mice. n = 5 mice/group.

(D) Amount of sIgA, as determined by enzyme-linked immunoassay (ELISA), in contents of the jejunum.

(E) Frequency of IgA-coated bacteria after staining of *Rag1*$^{-/-}$ feces with supernatant from WT and GATA4$^{\Delta IEC}$ jejunal contents. n = 4–5 mice/group.

(F) SFB loads, in jejunal mucosal scrapings of PBS-treated WT or GATA4$^{\Delta IEC}$ mice, and IgA-supplemented GATA4$^{\Delta IEC}$ mice. n = 5–7 mice/group.

(G) Heatmap of z-scored expression of region-specific GATA4-regulated genes in the KEGG retinol metabolism pathway, from RNA-seq on epithelial cells. Compared to other genes in the pathway expressed in epithelial samples, these genes are significantly enriched in GATA4-bound promoters, as determined by ChIP-seq (black squares in the annotation column) (Table S1; odds ratio 2.6, $p < 0.005$; Fisher exact test).

(H) Top, representative histogram of ALDH activity by ALDEFLUOR staining in jejunal epithelial cells. WT epithelial cells treated with ALDH inhibitor are shown as negative control for background fluorescence. Bottom, summary plots show the normalized geometric mean fluorescence intensity (gMFI) of ALDEFLUOR staining in epithelial cells from the jejunum and ileum of WT and GATA4$^{\Delta IEC}$ mice. n = 6 mice/group.

(I) Total IgA in the jejunal contents of WT, GATA4$^{\Delta IEC}$ vehicle-treated, and GATA4$^{\Delta IEC}$ RA-treated mice after 14 days. n = 4 mice/group.

(J) SFB loads, in jejunal mucosal scrapings of GF WT mice fed a control or vitamin A-deficient diet and subsequently colonized with SFB. n = 5 mice/group.

(K) *Pigr* expression as measured by qPCR relative to *Gapdh*, in the jejunum of WT and GATA4$^{\Delta IEC}$ mice. n = 7 mice/group.

All data in this figure are pooled from at least two-independent experiments and represented as mean ± SEM; ****$p < 0.0001$, ***$p < 0.001$, **$p < 0.01$, *$p < 0.05$, Kruskal-Wallis with Dunn multiple comparison test (B), ANOVA with Tukey multiple comparison test (C, F, H, I), t test (D, E, K), Mann Whitney test (J).

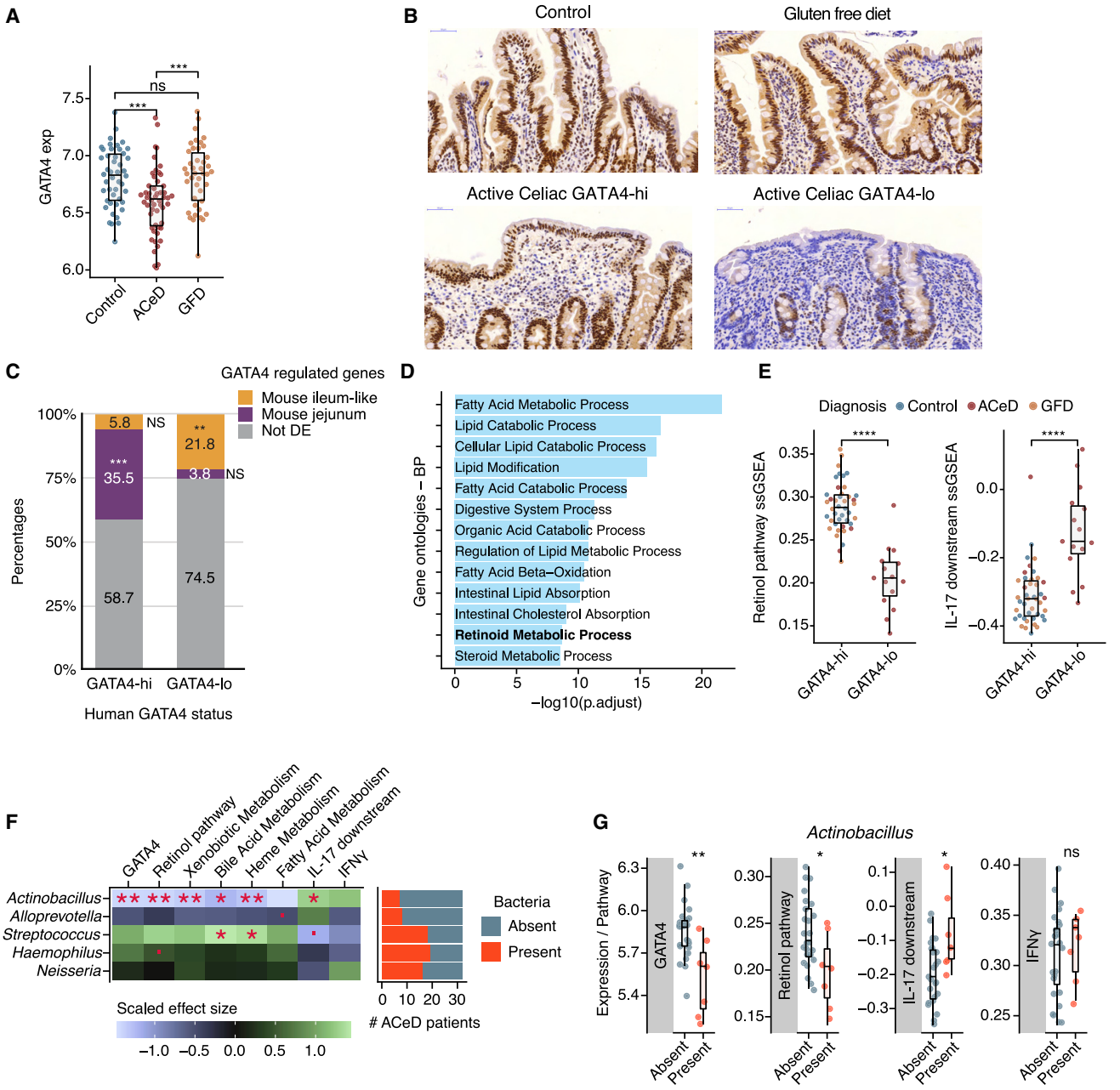

Figure 6. Loss of GATA4 expression is associated with lipid metabolic dysfunction and increased IL-17 signaling in celiac disease

(A) Normalized GATA4 expression in duodenal biopsies from healthy controls, active celiac disease patients (ACeD), and gluten-free-diet celiac patients (GFD).

(B) Representative IHC staining for GATA4 in healthy control, GATA4-hi, and GATA4-lo active celiac disease patients, and gluten-free-diet celiac patients.

(C) Bar plot shows the percentages of human-mouse homologous genes specific to GATA4-hi or GATA4-lo individuals, which are also either GATA4 regulated and specific to the jejunum (purple) or to the ileum-like tissues (yellow) or not (gray). ***$p < 10^{-51}$, **$p < 10^{-6}$, NS not significant.

(D) Bar plot shows the most significantly enriched gene ontologies and their significance (x axis, negative log FDR-adjusted p values) in the intersection of genes specific to GATA-hi individuals and WT mouse jejunum.

(E) Single-sample gene set enrichment analysis (ssGSEA) scores for the retinol metabolism (left) and IL-17 downstream signaling (right) pathways in GATA4-hi and GATA4-lo individuals from all patient groups.

(F) Left, heatmap displays the scaled effect size of the absence or presence of five relevant bacteria (Figure S4I) on GATA4 expression and on the ssGSEA scores of metabolic and immune pathways. Right, bar plot shows the numbers of detectable bacteria in ACeD samples.

(G) Boxplots show GATA4 expression and ssGSEA scores for the retinol metabolism, IL-17 downstream signaling, and IFN-γ pathways in ACeD patients, grouped by the absence or presence of *Actinobacillus*.

****$p < 0.0001$, ***$p < 0.001$, **$p < 0.01$, *$p < 0.05$, · $p < 0.1$, Wilcoxon rank test (A, E, G), Fisher exact test (C), and t test (F).

IL-17 signaling genes (Figures 6E and S6D–S6H). In fact, expression of both pathways was correlated (or anti-correlated, in the case of IL-17 signaling genes) with *GATA4* expression across all ACeD patients (Figures S6F and S6G). Together, these data reveal that loss of GATA4 expression in ACeD may play a role in regional defects, such as low retinol metabolism, low plasma cholesterol,[47] and increased IL-17 immunity. Several reports indicate that only a subset of ACeD patients have metabolic defects and that they are not directly correlated with the degree of villous atrophy.[42,48] Our results suggest that heterogeneity in levels of GATA4 expression may contribute to the heterogeneity in metabolic defects observed in ACeD patients.

Similarly, while the IL-17 signaling pathway was overall significantly more highly expressed in GATA4-lo versus GATA4-hi individuals, heterogeneity in its expression across GATA4-lo patients (Figure 6E) suggests that factors beyond loss of GATA4 expression contributed to Th17 cell responses in ACeD. In mice, the presence of Th17 cells in the ileum is dependent on the microbiota[11] and bacteria can drive distinct context-dependent immune responses.[49] To determine whether particular microbes were implicated in promoting IL-17 responses in ACeD patients, we leveraged a quantitative framework to detect absolute abundances of individual bacterial taxa in duodenal biopsies[50] along with concomitant host transcriptional analysis. Digital PCR anchoring of 16S rRNA amplicon sequencing revealed no change in overall bacterial load in ACeD patients versus controls (Figure S6I) and only a trend of stratification between ACeD patients and control in the second and third principal components (Figure S6J). We observed an expansion in ACeD patients of *Neisseria*, the only microbe with significant changes of abundance in the disease state (Figures S6K and S6L; Table S4), confirming a previous report.[51] Increased abundance of *Neisseria* was not, however, associated with decreased *GATA4* expression, metabolic defects, or IL-17 signaling in ACeD patients (Figure 6F; Table S5).

In contrast, we found that *Actinobacillus* was associated with lower *GATA4* expression, lower retinol metabolism, and higher IL-17 signaling in ACeD patients, but not controls (Figures 6F, 6G, and S6M; Table S5). We did not observe a significant association with the prototypical gluten-specific Th1 IFN-γ pathway in ACeD patients, suggesting that *Actinobacillus* may play a specific role in IL-17 immunity (Figures 6F and 6G). Intriguingly, *Actinobacillus* was also associated with other metabolic defects in ACeD patients, such as xenobiotic, bile acid, and heme metabolism, whereas other microbes, such as *Streptococcus,* had inverse patterns and positive associations with bile and heme metabolism (Figure 6F). These data also agree with the increased enrichment in IL-17 signaling genes in GATA4-lo ACeD patients but not controls.

The discovery of mucosal-associated bacteria, such as *Actinobacillus*, associated with the loss of GATA4, metabolic dysfunction, and IL-17 immunity in ACeD patients, highlights the potential importance of GATA4-dependent intestinal regionalization in the regulation of host microbial interactions and the pathogenesis of celiac disease.

DISCUSSION

In this report, we identified mechanisms controlling regionalization of the proximal and distal small intestine and revealed the importance of this segregation in homeostasis and disease. We found that by regulating retinol metabolism and local IgA responses, the epithelial transcription factor GATA4 limited the colonization of the proximal small intestine by the commensal SFB, which in turn restricted inflammatory immune responses. Both GATA4-deficient mice and GATA4-lo ACeD patients showed signs of microbiota-dependent dysregulated inflammatory T cell responses after infection or gluten ingestion, respectively. In particular, failure to restrict SFB colonization of the jejunum in GATA4$^{\Delta IEC}$ mice altered the immune response to the pathogen *C. rodentium* and promoted severe TNF-induced pathology and mortality. Furthermore, the intriguing association between loss of GATA4 expression in IECs, metabolic defects, and microbial-associated dysregulated IL-17 immune responses in ACeD patients poses the question of the role of GATA4 and IL-17 in regulating the severity of tissue damage and driving at least some of the clinical heterogeneity observed in ACeD patients. Beyond CeD, it raises the general question of whether a decrease in GATA4 in IECs of the proximal intestine, by altering host-microbial interactions and triggering dysregulated immune responses to bacteria, may play a role in other complex immune disorders. In contrast, the ileum, lacking GATA4 expression and producing less IgA, permits adherent microbes, such as SFB, to induce inflammatory IL-17^{+} T cell responses required for controlling pathogenic infections.[11,52] Therefore, there is a change in the tradeoff between the protective host immune responses (IgA) and inflammatory immune responses (IFN-γ and IL-17) in the proximal versus distal small intestine. Our work suggests that proper compartmentalization of epithelial programs and commensal bacteria colonization in the small intestine is critical for establishing immune homeostasis and preventing disease. Previous reports identified decreased IgA coating of fecal bacteria in celiac patients, and an increased prevalence of celiac disease in IgA-deficient patients.[53,54] Whether GATA4 deficiency drives this IgA defect in celiac patients remains to be investigated.

Another reason for bacterial and immune regionalization could be that the proximal small intestine evolved to maximize nutrient digestion and absorption to increase host fitness. Preventing adherent bacterial colonization and the development of inflammatory immune responses in the proximal small intestine may support these vital digestive functions. Together, our findings emphasize the need to integrate signals of regional changes in host cells and in commensal bacteria colonization to decipher the mechanisms underlying the development of complex immune disorders.

Limitations of the study

Here we find that GATA4 is an essential regulator of metabolic, immune, and microbial regionalization between the proximal and distal small intestine. To maintain this regionalization, GATA4 directly controls many biological pathways. While IgA was necessary and sufficient to control SFB colonization, retinol metabolism was not. Furthermore, supplementing retinoic acid to GATA4-deficient mice was not sufficient to fully restore luminal IgA to WT levels. Finally, we have evidence that GATA4 prevents *C. rodentium* from colonizing the proximal small intestine independently from IgA through yet unknown mechanisms. Together these data suggest that

other GATA4-dependent mechanisms are involved in regulating adherent bacteria colonization and luminal IgA, the identification of which will require future studies.

STAR★METHODS

Detailed methods are provided in the online version of this paper and include the following:

- KEY RESOURCES TABLE
- RESOURCE AVAILABILITY
  - Lead contact
  - Materials availability
  - Data and code availability
- EXPERIMENTAL MODEL AND SUBJECT DETAILS
  - Mice
  - Patients
  - *C. rodentium* infections
  - Microbial transfers
  - Vitamin A deficient diet
  - SFB TCRtg adoptive transfer
- METHOD DETAILS
  - Isolation of intestinal epithelial cells (IEC), intraepithelial lymphocytes (IEL), and lamina propria (LP) cells
  - Cytokine stimulation
  - Flow cytometry
  - DNA isolation
  - RNA isolation
  - qPCR
  - Histology
  - Transmission electron microscopy
  - ELISA
  - Luminal IgA isolation and *in vivo* treatment
  - In-vivo retinoic acid treatment
  - Bacterial staining with luminal IgA
  - Microbial 16S sequencing: Library generation and initial data processing
  - Microbial 16S sequencing: Absolute abundances
  - Microbial 16S sequencing data analysis: Poisson quality filtering
  - Microbial 16S sequencing data analysis: Statistical analysis
  - RNA-seq of purified IECs from mice
  - Tissue RNA-seq
  - Mouse RNA-seq data processing to obtain raw counts
  - Mouse RNA-seq data analysis: Quality control filtering and normalization
  - Mouse RNA-seq data analysis: Differential expression and gene set enrichment
  - Mouse RNA-seq data analysis: Data visualization
  - Annotation of GATA4-targeted genes
  - Generation of immune, IL-17, and IFNγ gene modules
  - Human RNA-seq data analysis
- QUANTIFICATION AND STATISTICAL ANALYSIS

SUPPLEMENTAL INFORMATION

Supplemental information can be found online at https://doi.org/10.1016/j.immuni.2022.12.009.

ACKNOWLEDGMENTS

We would like to thank the patients and their family members, as well as the University of Chicago Celiac Disease Center, for supporting our research. We would like to thank Drs. Sonia Kupfer, Carol Semrad, Ritu Verma, Hilary Jericho, and Ian Wilson from the Celiac Disease Center for consenting and recruiting patients. We would like to thank Joaquín Sanz Remón for his help with the general transcriptional analysis of celiac disease and control patient biopsies. We thank Drs. Kenya Honda and Gabriel Nuñez for providing rat SFB and ΔEAE *C. rodentium,* respectively. We thank Ivaylo Ivanov for providing SFB TCR transgenic mice and for helpful discussions. We thank Steven Erickson from Dr. Albert Bendelac's lab for generating IgA- and Jh-deficient mice using CRISPR-Cas technologies based on previously published mouse models.[24,55] We thank Betty Theriault, Kristin Kolar, and the entire Gnotobiotic Research Animal Facility at the University of Chicago for their help with the experiments involving gnotobiotic mice. We thank Yimei Chen and Tera Lavoie of the Advanced Electron Microscopy Core at University of Chicago for their help with transmission electron microscopy. We thank the Human Tissue Resource Center, the Integrated Light Microscopy Core Facility, Flow Cytometry Facility, and the Genomics Facility at the University of Chicago for their technical support. We thank Toufic Mayassi and Cezary Ciszewski for the thoughtful discussions and insightful comments. Finally, we thank Valerie Abadie for a critical reading of the manuscript and help with the graphical abstract. This work was supported by the National Institutes of Health via T32 AI007090 to Z.M.E., T32 GM007281 to D.G.S., U01AI109695 to A.M., U01 AI125250 to A.B., R01 AI144094 to A.B., R01DK103761 to N.S., R01 DK067180 to B.J., and the Digestive Diseases Research Core Center C-IID P30 DK42086 at the University of Chicago to B.J.

AUTHOR CONTRIBUTIONS

Z.M.E. and B.J. conceived the study and designed the experiments. S.J.R. designed and oversaw computational analysis of the RNA-seq data with input from Z.M.E., B.J., J.J.S., and R.A.-G. Based on their previously published work and studies performed in gnotobiotic mice, N.S., A.M., and P.M. put forward the concept that absence of GATA4 in epithelial cells was driving inflammatory immune responses in the jejunum in a microbiota-dependent manner. Z.M.E., W.L., A.K., D.G.S., J.D.E., and J.T.B. performed the experiments. Z.M.E., W.L., J.J.S, R.A.-G., J.T.B., and S.J.R. analyzed and interpreted the data. J.J.S. performed computational analysis of mouse RNA-seq data, and R.A.-G. performed computational analysis of human RNA-seq data. J.T.B. performed the 16S sequencing and analysis. D.G.S. and V.D. created the RNA-seq libraries, and S.G. performed the DNA alignments. P.M. supervised an initial microarray transcriptional analysis. I.L.T contributed to and L.B.B. supervised RNA-seq analysis of human celiac disease patients. R.F.I. supervised the 16S analysis. A.B. supervised the IgA experiments. Z.M.E., S.J.R., and B.J. wrote the manuscript. W.L., J.J.S, J.T.B., R.F.I., A.M., N.S., and A.B. edited the manuscript. R.F.I., A.M., A.B., N.S., and B.J. acquired funds to support the work, and B.J. directed the study.

DECLARATION OF INTERESTS

The authors declare no competing interests.

INCLUSION AND DIVERSITY

We support inclusive, diverse, and equitable conduct of research.

Received: September 15, 2022
Revised: November 16, 2022
Accepted: December 12, 2022
Published: January 10, 2023

REFERENCES

1. Mowat, A.M., and Agace, W.W. (2014). Regional specialization within the intestinal immune system. Nat. Rev. Immunol. *14*, 667–685. https://doi.org/10.1038/nri3738.

2. Donaldson, G.P., Lee, S.M., and Mazmanian, S.K. (2016). Gut biogeography of the bacterial microbiota. Nat. Rev. Microbiol. *14*, 20–32. https://doi.org/10.1038/nrmicro3552.
3. Esterházy, D., Canesso, M.C.C., Mesin, L., Muller, P.A., de Castro, T.B.R., Lockhart, A., ElJalby, M., Faria, A.M.C., and Mucida, D. (2019). Compartmentalized gut lymph node drainage dictates adaptive immune responses. Nature *569*, 126–130. https://doi.org/10.1038/s41586-019-1125-3.
4. Bosse, T., Piaseckyj, C.M., Burghard, E., Fialkovich, J.J., Rajagopal, S., Pu, W.T., and Krasinski, S.D. (2006). Gata4 is essential for the maintenance of jejunal-ileal identities in the adult mouse small intestine. Mol. Cell Biol. *26*, 9060–9070. https://doi.org/10.1128/mcb.00124-06.
5. Battle, M.A., Bondow, B.J., Iverson, M.A., Adams, S.J., Jandacek, R.J., Tso, P., and Duncan, S.A. (2008). GATA4 is essential for jejunal function in mice. Gastroenterology *135*, 1676–1686.e1. https://doi.org/10.1053/j.gastro.2008.07.074.
6. Bhattacharya, S., Dunn, P., Thomas, C.G., Smith, B., Schaefer, H., Chen, J., Hu, Z., Zalocusky, K.A., Shankar, R.D., Shen-Orr, S.S., et al. (2018). ImmPort, toward repurposing of open access immunological assay data for translational and clinical research. Sci. Data *5*, 180015. https://doi.org/10.1038/sdata.2018.15.
7. Kelley, J., de Bono, B., and Trowsdale, J. (2005). IRIS: a database surveying known human immune system genes. Genomics *85*, 503–511. https://doi.org/10.1016/j.ygeno.2005.01.009.
8. Lee, J.Y., Hall, J.A., Kroehling, L., Wu, L., Najar, T., Nguyen, H.H., Lin, W.Y., Yeung, S.T., Silva, H.M., Li, D., et al. (2020). Serum amyloid a proteins induce pathogenic Th17 cells and promote inflammatory disease. Cell *180*, 79–91.e16. https://doi.org/10.1016/j.cell.2019.11.026.
9. Thompson, C.A., Wojta, K., Pulakanti, K., Rao, S., Dawson, P., and Battle, M.A. (2017). GATA4 is sufficient to establish jejunal versus ileal identity in the small intestine. Cell. Mol. Gastroenterol. Hepatol. *3*, 422–446. https://doi.org/10.1016/j.jcmgh.2016.12.009.
10. Aronson, B.E., Rabello Aronson, S., Berkhout, R.P., Chavoushi, S.F., He, A., Pu, W.T., Verzi, M.P., and Krasinski, S.D. (2014). GATA4 represses an ileal program of gene expression in the proximal small intestine by inhibiting the acetylation of histone H3, lysine 27. Biochim. Biophys. Acta *1839*, 1273–1282. https://doi.org/10.1016/j.bbagrm.2014.05.018.
11. Ivanov, I.I., Atarashi, K., Manel, N., Brodie, E.L., Shima, T., Karaoz, U., Wei, D., Goldfarb, K.C., Santee, C.A., Lynch, S.V., et al. (2009). Induction of intestinal Th17 cells by segmented filamentous bacteria. Cell *139*, 485–498. https://doi.org/10.1016/j.cell.2009.09.033.
12. Yang, Y., Torchinsky, M.B., Gobert, M., Xiong, H., Xu, M., Linehan, J.L., Alonzo, F., Ng, C., Chen, A., Lin, X., et al. (2014). Focused specificity of intestinal TH17 cells towards commensal bacterial antigens. Nature *510*, 152–156. https://doi.org/10.1038/nature13279.
13. Herp, S., Durai Raj, A.C., Salvado Silva, M., Woelfel, S., and Stecher, B. (2021). The human symbiont Mucispirillum schaedleri: causality in health and disease. Med. Microbiol. Immunol. *210*, 173–179. https://doi.org/10.1007/s00430-021-00702-9.
14. Atarashi, K., Tanoue, T., Ando, M., Kamada, N., Nagano, Y., Narushima, S., Suda, W., Imaoka, A., Setoyama, H., Nagamori, T., et al. (2015). Th17 cell induction by adhesion of microbes to intestinal epithelial cells. Cell *163*, 367–380. https://doi.org/10.1016/j.cell.2015.08.058.
15. Prakash, T., Oshima, K., Morita, H., Fukuda, S., Imaoka, A., Kumar, N., Sharma, V.K., Kim, S.W., Takahashi, M., Saitou, N., et al. (2011). Complete genome sequences of rat and mouse segmented filamentous bacteria, a potent inducer of th17 cell differentiation. Cell Host Microbe *10*, 273–284. https://doi.org/10.1016/j.chom.2011.08.007.
16. Kamada, N., Kim, Y.G., Sham, H.P., Vallance, B.A., Puente, J.L., Martens, E.C., and Núñez, G. (2012). Regulated virulence controls the ability of a pathogen to compete with the gut microbiota. Science *336*, 1325–1329. https://doi.org/10.1126/science.1222195.
17. Collins, J.W., Keeney, K.M., Crepin, V.F., Rathinam, V.A.K., Fitzgerald, K.A., Finlay, B.B., and Frankel, G. (2014). Citrobacter rodentium: infection, inflammation and the microbiota. Nat. Rev. Microbiol. *12*, 612–623. https://doi.org/10.1038/nrmicro3315.
18. Ma, T.Y., Iwamoto, G.K., Hoa, N.T., Akotia, V., Pedram, A., Boivin, M.A., and Said, H.M. (2004). TNF-alpha-induced increase in intestinal epithelial tight junction permeability requires NF-kappa B activation. Am. J. Physiol. Gastrointest. Liver Physiol. *286*, G367–G376. https://doi.org/10.1152/ajpgi.00173.
19. Turner, J.R. (2006). Molecular basis of epithelial barrier regulation: from basic mechanisms to clinical application. Am. J. Pathol. *169*, 1901–1909. https://doi.org/10.2353/ajpath.2006.060681.
20. Suenaert, P., Bulteel, V., Lemmens, L., Noman, M., Geypens, B., Van Assche, G., Geboes, K., Ceuppens, J.L., and Rutgeerts, P. (2002). Anti-tumor necrosis factor treatment restores the gut barrier in Crohn's disease. Am. J. Gastroenterol. *97*, 2000–2004. https://doi.org/10.1111/j.1572-0241.2002.05914.x.
21. Simmons, C.P., Goncalves, N.S., Ghaem-Maghami, M., Bajaj-Elliott, M., Clare, S., Neves, B., Frankel, G., Dougan, G., and MacDonald, T.T. (2002). Impaired resistance and enhanced pathology during infection with a noninvasive, attaching-effacing enteric bacterial pathogen, Citrobacter rodentium, in mice lacking IL-12 or IFN-gamma. J. Immunol. *168*, 1804–1812. https://doi.org/10.4049/jimmunol.168.4.1804.
22. Matsunaga, Y., Clark, T., Wanek, A.G., Bitoun, J.P., Gong, Q., Good, M., and Kolls, J.K. (2021). Intestinal IL-17R signaling controls secretory IgA and oxidase balance in citrobacter rodentium Infection. J. Immunol. *206*, 766–775. https://doi.org/10.4049/jimmunol.2000591.
23. Shulzhenko, N., Morgun, A., Hsiao, W., Battle, M., Yao, M., Gavrilova, O., Orandle, M., Mayer, L., Macpherson, A.J., McCoy, K.D., et al. (2011). Crosstalk between B lymphocytes, microbiota and the intestinal epithelium governs immunity versus metabolism in the gut. Nat. Med. *17*, 1585–1593. https://doi.org/10.1038/nm.2505.
24. Chen, J., Trounstine, M., Alt, F.W., Young, F., Kurahara, C., Loring, J.F., and Huszar, D. (1993). Immunoglobulin gene rearrangement in B cell deficient mice generated by targeted deletion of the JH locus. Int. Immunol. *5*, 647–656. https://doi.org/10.1093/intimm/5.6.647.
25. Bunker, J.J., Erickson, S.A., Flynn, T.M., Henry, C., Koval, J.C., Meisel, M., Jabri, B., Antonopoulos, D.A., Wilson, P.C., and Bendelac, A. (2017). Natural polyreactive IgA antibodies coat the intestinal microbiota. Science *358*, eaan6619. https://doi.org/10.1126/science.aan6619.
26. Bunker, J.J., Flynn, T.M., Koval, J.C., Shaw, D.G., Meisel, M., McDonald, B.D., Ishizuka, I.E., Dent, A.L., Wilson, P.C., Jabri, B., et al. (2015). Innate and adaptive humoral responses coat distinct commensal bacteria with immunoglobulin A. Immunity *43*, 541–553. https://doi.org/10.1016/j.immuni.2015.08.007.
27. Palm, N.W., de Zoete, M.R., Cullen, T.W., Barry, N.A., Stefanowski, J., Hao, L., Degnan, P.H., Hu, J., Peter, I., Zhang, W., et al. (2014). Immunoglobulin A coating identifies colitogenic bacteria in inflammatory bowel disease. Cell *158*, 1000–1010. https://doi.org/10.1016/j.cell.2014.08.006.
28. Donaldson, G.P., Ladinsky, M.S., Yu, K.B., Sanders, J.G., Yoo, B.B., Chou, W.C., Conner, M.E., Earl, A.M., Knight, R., Bjorkman, P.J., and Mazmanian, S.K. (2018). Gut microbiota utilize immunoglobulin A for mucosal colonization. Science *360*, 795–800. https://doi.org/10.1126/science.aaq0926.
29. Kamada, N., Sakamoto, K., Seo, S.U., Zeng, M.Y., Kim, Y.G., Cascalho, M., Vallance, B.A., Puente, J.L., and Núñez, G. (2015). Humoral immunity in the gut selectively targets phenotypically virulent attaching-and-effacing bacteria for intraluminal elimination. Cell Host Microbe *17*, 617–627. https://doi.org/10.1016/j.chom.2015.04.001.
30. Goncalves, A., Roi, S., Nowicki, M., Dhaussy, A., Huertas, A., Amiot, M.J., and Reboul, E. (2015). Fat-soluble vitamin intestinal absorption: absorption sites in the intestine and interactions for absorption. Food Chem. *172*, 155–160. https://doi.org/10.1016/j.foodchem.2014.09.021.
31. Herr, F.M., Wardlaw, S.A., Kakkad, B., Albrecht, A., Quick, T.C., and Ong, D.E. (1993). Intestinal vitamin A metabolism: coordinate distribution of enzymes and CRBP(II). J. Lipid Res. *34*, 1545–1554.
32. Mora, J.R., Iwata, M., Eksteen, B., Song, S.Y., Junt, T., Senman, B., Otipoby, K.L., Yokota, A., Takeuchi, H., Ricciardi-Castagnoli, P., et al. (2006).

Generation of gut-homing IgA-secreting B cells by intestinal dendritic cells. Science *314*, 1157–1160. https://doi.org/10.1126/science.1132742.

33. Jijon, H.B., Suarez-Lopez, L., Diaz, O.E., Das, S., De Calisto, J., Paradakusz, M., Yaffe, M.B., Pittet, M.J., Mora, J.R., Belkaid, Y., et al. (2018). Intestinal epithelial cell-specific RARα depletion results in aberrant epithelial cell homeostasis and underdeveloped immune system. Mucosal Immunol. *11*, 703–715. https://doi.org/10.1038/mi.2017.91.
34. Gattu, S., Bang, Y.-J., Pendse, M., Dende, C., Chara, A.L., Harris, T.A., Wang, Y., Ruhn, K.A., Kuang, Z., Sockanathan, S., and Hooper, L.V. (2019). Epithelial retinoic acid receptor β regulates serum amyloid A expression and vitamin A-dependent intestinal immunity. Proc. Natl. Acad. Sci. USA *116*, 10911–10916. https://doi.org/10.1073/pnas.1812069116.
35. Johansen, F.E., and Kaetzel, C.S. (2011). Regulation of the polymeric immunoglobulin receptor and IgA transport: new advances in environmental factors that stimulate pIgR expression and its role in mucosal immunity. Mucosal Immunol. *4*, 598–602. https://doi.org/10.1038/mi.2011.37.
36. Jabri, B., and Sollid, L.M. (2009). Tissue-mediated control of immunopathology in coeliac disease. Nat. Rev. Immunol. *9*, 858–870. https://doi.org/10.1038/nri2670.
37. Monteleone, I., Sarra, M., Del Vecchio Blanco, G., Paoluzi, O.A., Franzè, E., Fina, D., Fabrizi, A., MacDonald, T.T., Pallone, F., and Monteleone, G. (2010). Characterization of IL-17A-producing cells in celiac disease mucosa. J. Immunol. *184*, 2211–2218. https://doi.org/10.4049/jimmunol.0901919.
38. Castellanos-Rubio, A., Santin, I., Irastorza, I., Castaño, L., Carlos Vitoria, J., and Ramon Bilbao, J. (2009). TH17 (and TH1) signatures of intestinal biopsies of CD patients in response to gliadin. Autoimmunity *42*, 69–73. https://doi.org/10.1080/08916930802350789.
39. Bodd, M., Ráki, M., Tollefsen, S., Fallang, L.E., Bergseng, E., Lundin, K.E.A., and Sollid, L.M. (2010). HLA-DQ2-restricted gluten-reactive T cells produce IL-21 but not IL-17 or IL-22. Mucosal Immunol. *3*, 594–601. https://doi.org/10.1038/mi.2010.36.
40. Mayassi, T., Ladell, K., Gudjonson, H., McLaren, J.E., Shaw, D.G., Tran, M.T., Rokicka, J.J., Lawrence, I., Grenier, J.C., van Unen, V., et al. (2019). Chronic inflammation permanently reshapes tissue-resident immunity in celiac disease. Cell *176*, 967–981.e19. https://doi.org/10.1016/j.cell.2018.12.039.
41. Brar, P., Kwon, G.Y., Holleran, S., Bai, D., Tall, A.R., Ramakrishnan, R., and Green, P.H.R. (2006). Change in lipid profile in celiac disease: beneficial effect of gluten-free diet. Am. J. Med. *119*, 786–790. https://doi.org/10.1016/j.amjmed.2005.12.025.
42. Bledsoe, A.C., King, K.S., Larson, J.J., Snyder, M., Absah, I., Choung, R.S., and Murray, J.A. (2019). Micronutrient deficiencies are common in contemporary celiac disease despite lack of overt malabsorption symptoms. Mayo Clin. Proc. *94*, 1253–1260. https://doi.org/10.1016/j.mayocp.2018.11.036.
43. Caminero, A., McCarville, J.L., Galipeau, H.J., Deraison, C., Bernier, S.P., Constante, M., Rolland, C., Meisel, M., Murray, J.A., Yu, X.B., et al. (2019). Duodenal bacterial proteolytic activity determines sensitivity to dietary antigen through protease-activated receptor-2. Nat. Commun. *10*, 1198. https://doi.org/10.1038/s41467-019-09037-9.
44. Cenit, M.C., Olivares, M., Codoñer-Franch, P., and Sanz, Y. (2015). Intestinal microbiota and celiac disease: cause, consequence or co-evolution? Nutrients *7*, 6900–6923. https://doi.org/10.3390/nu7085314.
45. Abadie, V., Kim, S.M., Lejeune, T., Palanski, B.A., Ernest, J.D., Tastet, O., Voisine, J., Discepolo, V., Marietta, E.V., Hawash, M.B.F., et al. (2020). IL-15, gluten and HLA-DQ8 drive tissue destruction in coeliac disease. Nature *578*, 600–604. https://doi.org/10.1038/s41586-020-2003-8.
46. Taavela, J., Viiri, K., Popp, A., Oittinen, M., Dotsenko, V., Peräaho, M., Staff, S., Sarin, J., Leon, F., Mäki, M., and Isola, J. (2019). Histological, immunohistochemical and mRNA gene expression responses in coeliac disease patients challenged with gluten using PAXgene fixed paraffin-embedded duodenal biopsies. BMC Gastroenterol. *19*, 189. https://doi.org/10.1186/s12876-019-1089-7.
47. Vuoristo, M., Kesäniemi, Y.A., Gylling, H., and Miettinen, T.A. (1993). Metabolism of cholesterol and apolipoprotein B in celiac disease. Metabolism *42*, 1386–1391. https://doi.org/10.1016/0026-0495(93)90187-s.
48. Kemppainen, T.A., Kosma, V.M., Janatuinen, E.K., Julkunen, R.J., Pikkarainen, P.H., and Uusitupa, M.I. (1998). Nutritional status of newly diagnosed celiac disease patients before and after the institution of a celiac disease diet–association with the grade of mucosal villous atrophy. Am. J. Clin. Nutr. *67*, 482–487. https://doi.org/10.1093/ajcn/67.3.482.
49. Xu, M., Pokrovskii, M., Ding, Y., Yi, R., Au, C., Harrison, O.J., Galan, C., Belkaid, Y., Bonneau, R., and Littman, D.R. (2018). c-MAF-dependent regulatory T cells mediate immunological tolerance to a gut pathobiont. Nature *554*, 373–377. https://doi.org/10.1038/nature25500.
50. Barlow, J.T., Bogatyrev, S.R., and Ismagilov, R.F. (2020). A quantitative sequencing framework for absolute abundance measurements of mucosal and lumenal microbial communities. Nat. Commun. *11*, 2590. https://doi.org/10.1038/s41467-020-16224-6.
51. D'Argenio, V., Casaburi, G., Precone, V., Pagliuca, C., Colicchio, R., Sarnataro, D., Discepolo, V., Kim, S.M., Russo, I., Del Vecchio Blanco, G., et al. (2016). Metagenomics Reveals Dysbiosis and a Potentially Pathogenic N. flavescens Strain in Duodenum of Adult Celiac Patients. Am. J. Gastroenterol. *111*, 879–890. https://doi.org/10.1038/ajg.2016.95.
52. Shi, Z., Zou, J., Zhang, Z., Zhao, X., Noriega, J., Zhang, B., Zhao, C., Ingle, H., Bittinger, K., Mattei, L.M., et al. (2019). Segmented filamentous bacteria prevent and cure rotavirus infection. Cell *179*, 644–658.e13. https://doi.org/10.1016/j.cell.2019.09.028.
53. De Palma, G., Nadal, I., Medina, M., Donat, E., Ribes-Koninckx, C., Calabuig, M., and Sanz, Y. (2010). Intestinal dysbiosis and reduced immunoglobulin-coated bacteria associated with coeliac disease in children. BMC Microbiol. *10*, 63. https://doi.org/10.1186/1471-2180-10-63.
54. Kumar, V., Jarzabek-Chorzelska, M., Sulej, J., Karnewska, K., Farrell, T., and Jablonska, S. (2002). Celiac disease and immunoglobulin a deficiency: how effective are the serological methods of diagnosis? Clin. Diagn. Lab. Immunol. *9*, 1295–1300. https://doi.org/10.1128/cdli.9.6.1295-1300.2002.
55. Harriman, G.R., Bogue, M., Rogers, P., Finegold, M., Pacheco, S., Bradley, A., Zhang, Y., and Mbawuike, I.N. (1999). Targeted deletion of the IgA constant region in mice leads to IgA deficiency with alterations in expression of other Ig isotypes. J. Immunol. *162*, 2521–2529.
56. Pickard, J.M., Maurice, C.F., Kinnebrew, M.A., Abt, M.C., Schenten, D., Golovkina, T.V., Bogatyrev, S.R., Ismagilov, R.F., Pamer, E.G., Turnbaugh, P.J., and Chervonsky, A.V. (2014). Rapid fucosylation of intestinal epithelium sustains host-commensal symbiosis in sickness. Nature *514*, 638–641. https://doi.org/10.1038/nature13823.
57. Klose, C.S.N., Flach, M., Möhle, L., Rogell, L., Hoyler, T., Ebert, K., Fabiunke, C., Pfeifer, D., Sexl, V., Fonseca-Pereira, D., et al. (2014). Differentiation of type 1 ILCs from a common progenitor to all helper-like innate lymphoid cell lineages. Cell *157*, 340–356. https://doi.org/10.1016/j.cell.2014.03.030.
58. Sano, T., Huang, W., Hall, J.A., Yang, Y., Chen, A., Gavzy, S.J., Lee, J.Y., Ziel, J.W., Miraldi, E.R., Domingos, A.I., et al. (2015). An IL-23R/IL-22 circuit regulates epithelial serum amyloid A to promote local effector Th17 responses. Cell *163*, 381–393. https://doi.org/10.1016/j.cell.2015.08.061.
59. Deloris Alexander, A., Orcutt, R.P., Henry, J.C., Baker, J., Jr., Bissahoyo, A.C., and Threadgill, D.W. (2006). Quantitative PCR assays for mouse enteric flora reveal strain-dependent differences in composition that are influenced by the microenvironment. Mamm. Genome *17*, 1093–1104. https://doi.org/10.1007/s00335-006-0063-1.
60. Sagaidak, S., Taibi, A., Wen, B., and Comelli, E.M. (2016). Development of a real-time PCR assay for quantification of Citrobacter rodentium. J. Microbiol. Methods *126*, 76–77. https://doi.org/10.1016/j.mimet.2016.05.008.
61. Amann, R.I., Binder, B.J., Olson, R.J., Chisholm, S.W., Devereux, R., and Stahl, D.A. (1990). Combination of 16S rRNA-targeted oligonucleotide probes with flow cytometry for analyzing mixed microbial populations. Appl. Environ. Microbiol. *56*, 1919–1925. https://doi.org/10.1128/aem.56.6.1919-1925.1990.

62. Tsai, P.Y., Zhang, B., He, W.Q., Zha, J.M., Odenwald, M.A., Singh, G., Tamura, A., Shen, L., Sailer, A., Yeruva, S., et al. (2017). IL-22 upregulates epithelial claudin-2 to drive diarrhea and enteric pathogen clearance. Cell Host Microbe *21*, 671–681.e4. https://doi.org/10.1016/j.chom.2017.05.009.

63. Bolyen, E., Rideout, J.R., Dillon, M.R., Bokulich, N.A., Abnet, C.C., Al-Ghalith, G.A., Alexander, H., Alm, E.J., Arumugam, M., Asnicar, F., et al. (2019). Reproducible, interactive, scalable and extensible microbiome data science using QIIME 2. Nat. Biotechnol. *37*, 852–857. https://doi.org/10.1038/s41587-019-0209-9.

64. Quast, C., Pruesse, E., Yilmaz, P., Gerken, J., Schweer, T., Yarza, P., Peplies, J., and Glöckner, F.O. (2013). The SILVA ribosomal RNA gene database project: improved data processing and web-based tools. Nucleic Acids Res. *41*, D590–D596. https://doi.org/10.1093/nar/gks1219.

65. Husby, S., Koletzko, S., Korponay-Szabó, I.R., Mearin, M.L., Phillips, A., Shamir, R., Troncone, R., Giersiepen, K., Branski, D., Catassi, C., et al. (2012). European society for pediatric gastroenterology, hepatology, and nutrition guidelines for the diagnosis of coeliac disease. J. Pediatr. Gastroenterol. Nutr. *54*, 136–160.

66. Molloy, M.J., Grainger, J.R., Bouladoux, N., Hand, T.W., Koo, L.Y., Naik, S., Quinones, M., Dzutsev, A.K., Gao, J.L., Trinchieri, G., et al. (2013). Intraluminal containment of commensal outgrowth in the gut during infection-induced dysbiosis. Cell Host Microbe *14*, 318–328. https://doi.org/10.1016/j.chom.2013.08.003.

67. Lefrançois, L., and Lycke, N. (2001). Isolation of mouse small intestinal intraepithelial lymphocytes, Peyer's patch, and lamina propria cells. Curr. Protoc. Immunol. *Chapter 3*. Unit 3.19. https://doi.org/10.1002/0471142735.im0319s17.

68. Earley, Z.M., Akhtar, S., Green, S.J., Naqib, A., Khan, O., Cannon, A.R., Hammer, A.M., Morris, N.L., Li, X., Eberhardt, J.M., et al. (2015). Burn injury alters the intestinal microbiome and increases gut permeability and bacterial translocation. PLoS One *10*, e0129996. https://doi.org/10.1371/journal.pone.0129996.

69. Bogatyrev, S.R., and Ismagilov, R.F. (2020). Quantitative microbiome profiling in lumenal and tissue samples with broad coverage and dynamic range via a single-step 16S rRNA gene DNA copy quantification and amplicon barcoding. Preprint at bioRxiv. https://doi.org/10.1101/2020.01.22.914705.

70. Bogatyrev, S.R., Rolando, J.C., and Ismagilov, R.F. (2020). Self-reinoculation with fecal flora changes microbiota density and composition leading to an altered bile-acid profile in the mouse small intestine. Microbiome *8*, 19. https://doi.org/10.1186/s40168-020-0785-4.

71. Weiss, S., Xu, Z.Z., Peddada, S., Amir, A., Bittinger, K., Gonzalez, A., Lozupone, C., Zaneveld, J.R., Vázquez-Baeza, Y., Birmingham, A., et al. (2017). Normalization and microbial differential abundance strategies depend upon data characteristics. Microbiome *5*, 27. https://doi.org/10.1186/s40168-017-0237-y.

72. Barlow, J.T., Leite, G., Romano, A.E., Sedighi, R., Chang, C., Celly, S., Rezaie, A., Mathur, R., Pimentel, M., and Ismagilov, R.F. (2021). Quantitative sequencing clarifies the role of disruptor taxa, oral microbiota, and strict anaerobes in the human small-intestine microbiome. Microbiome *9*, 214. https://doi.org/10.1186/s40168-021-01162-2.

73. Bourgey, M., Dali, R., Eveleigh, R., Chen, K.C., Letourneau, L., Fillon, J., Michaud, M., Caron, M., Sandoval, J., Lefebvre, F., et al. (2019). GenPipes: an open-source framework for distributed and scalable genomic analyses. GigaScience *8*, giz037. https://doi.org/10.1093/gigascience/giz037.

74. Bolger, A.M., Lohse, M., and Usadel, B. (2014). Trimmomatic: a flexible trimmer for Illumina sequence data. Bioinformatics *30*, 2114–2120. https://doi.org/10.1093/bioinformatics/btu170.

75. Dobin, A., Davis, C.A., Schlesinger, F., Drenkow, J., Zaleski, C., Jha, S., Batut, P., Chaisson, M., and Gingeras, T.R. (2013). STAR: ultrafast universal RNA-seq aligner. Bioinformatics *29*, 15–21. https://doi.org/10.1093/bioinformatics/bts635.

76. Anders, S., Pyl, P.T., and Huber, W. (2015). HTSeq–a Python framework to work with high-throughput sequencing data. Bioinformatics *31*, 166–169. https://doi.org/10.1093/bioinformatics/btu638.

77. Love, M.I., Huber, W., and Anders, S. (2014). Moderated estimation of fold change and dispersion for RNA-seq data with DESeq2. Genome Biol. *15*, 550. https://doi.org/10.1186/s13059-014-0550-8.

78. Ritchie, M.E., Phipson, B., Wu, D., Hu, Y., Law, C.W., Shi, W., and Smyth, G.K. (2015). limma powers differential expression analyses for RNA-sequencing and microarray studies. Nucleic Acids Res. *43*, e47. https://doi.org/10.1093/nar/gkv007.

79. Korotkevich, G., Sukhov, V., Budin, N., Shpak, B., Artyomov, M.N., and Sergushichev, A. (2021). Fast gene set enrichment analysis. Preprint at bioRxiv060012. https://doi.org/10.1101/060012.

80. Mouse Genome Sequencing Consortium, Waterston, R.H., Lindblad-Toh, K., Birney, E., Rogers, J., Abril, J.F., Agarwal, P., Agarwala, R., Ainscough, R., Alexandersson, M., et al. (2002). Initial sequencing and comparative analysis of the mouse genome. Nature *420*, 520–562. https://doi.org/10.1038/nature01262.

81. Ashburner, M., Ball, C.A., Blake, J.A., Botstein, D., Butler, H., Cherry, J.M., Davis, A.P., Dolinski, K., Dwight, S.S., Eppig, J.T., et al. (2000). Gene ontology: tool for the unification of biology. The Gene Ontology Consortium. Nat. Genet. *25*, 25–29. https://doi.org/10.1038/75556.

82. Gene Ontology Consortium (2021). The gene ontology resource: enriching a GOld mine. Nucleic Acids Res. *49*. D325–d334. https://doi.org/10.1093/nar/gkaa1113.

83. Blighe, K. (2021). PCAtools: everything principal component analysis. https://github.com/kevinblighe/PCAtools.

84. Gu, Z., Eils, R., and Schlesner, M. (2016). Complex heatmaps reveal patterns and correlations in multidimensional genomic data. Bioinformatics *32*, 2847–2849. https://doi.org/10.1093/bioinformatics/btw313.

85. Kumar, P., Monin, L., Castillo, P., Elsegeiny, W., Horne, W., Eddens, T., Vikram, A., Good, M., Schoenborn, A.A., Bibby, K., et al. (2016). Intestinal Interleukin-17 Receptor Signaling Mediates Reciprocal Control of the Gut Microbiota and Autoimmune Inflammation. Immunity *44*, 659–671. https://doi.org/10.1016/j.immuni.2016.02.007.

86. Liu, S.Y., Sanchez, D.J., Aliyari, R., Lu, S., and Cheng, G. (2012). Systematic identification of type I and type II interferon-induced antiviral factors. Proc. Natl. Acad. Sci. USA *109*, 4239–4244. https://doi.org/10.1073/pnas.1114981109.

87. Benci, J.L., Xu, B., Qiu, Y., Wu, T.J., Dada, H., Twyman-Saint Victor, C., Cucolo, L., Lee, D.S.M., Pauken, K.E., Huang, A.C., et al. (2016). Tumor interferon signaling regulates a multigenic resistance program to immune checkpoint blockade. Cell *167*, 1540–1554.e12. https://doi.org/10.1016/j.cell.2016.11.022.

88. Bray, N.L., Pimentel, H., Melsted, P., and Pachter, L. (2016). Near-optimal probabilistic RNA-seq quantification. Nat. Biotechnol. *34*, 525–527. https://doi.org/10.1038/nbt.3519.

89. Yu, G., Wang, L.G., Han, Y., and He, Q.Y. (2012). clusterProfiler: an R package for comparing biological themes among gene clusters. OMICS *16*, 284–287. https://doi.org/10.1089/omi.2011.0118.

90. Liberzon, A., Birger, C., Thorvaldsdóttir, H., Ghandi, M., Mesirov, J.P., and Tamayo, P. (2015). The Molecular Signatures Database (MSigDB) hallmark gene set collection. Cell Syst. *1*, 417–425. https://doi.org/10.1016/j.cels.2015.12.004.

91. Hänzelmann, S., Castelo, R., and Guinney, J. (2013). GSVA: gene set variation analysis for microarray and RNA-seq data. BMC Bioinf. *14*, 7. https://doi.org/10.1186/1471-2105-14-7.

STAR★METHODS

KEY RESOURCES TABLE

REAGENT or RESOURCE	SOURCE	IDENTIFIER
Antibodies		
CD45 Pac Blue (30-F11)	Biolegend	Cat#103126; RRID: AB_493535
TCRgd FITC (eBioGL3)	Thermo Fisher	Cat#11-5711-82; RRID: AB_465238
CD4 BV785 (GK1.5)	Biolegend	Cat#100453; RRID: AB_2565843
CD4 BV605 (GK1.5)	Biolegend	Cat#100451; RRID: AB_2564591
CD8β BUV395 (H35–17.2)	BD	Cat#740278; RRID: AB_2740017
CD8α PerCp/Cy5.5 (53-6.7)	BD	Cat#551162; RRID: AB_394081
NK1.1 PE-CF594 (PK136)	BD	Cat#562864; RRID: AB_2737850
TCRβ BUV737 (H57-597)	BD	Cat#612821; RRID: AB_2870145
TCRβ BV711 (H57-597)	BD	Cat#563135; RRID: AB_2738023
CD3ε BUV737 (145-2C11)	BD	Cat#612771; RRID: AB_2870100
IFNγ APC (XMG1.2)	BD	Cat#554413; RRID: AB_398551
TNF BB700 (MP6-XT22)	BD	Cat#566510; RRID: AB_2869775
IL10 PEcy7 (JES5-16E3)	Biolegend	Cat#505026; RRID: AB_11150582
IL17a PE (ebio17B7)	Thermo Fisher	Cat#12-7177-81; RRID: AB_763582
CD45.1 Pac Blue (A20)	Biolegend	Cat#110722; RRID: AB_492866
CD45.2 BUV395 (104)	BD	Cat#553772; RRID: AB_395041
vβ14 TCR FITC (14-2)	BD	Cat#553258; RRID: AB_394738
RORγt BV786 (Q31-37)	BD	Cat#564723; RRID: AB_2738916
FOXP3 eflour450 (FJK-16s)	Thermo Fisher	Cat#48-5773-82; RRID: AB_1518812
FOXP3 FITC (FJK-16s)	Thermo Fisher	Cat#11-5773-82; RRID: AB_465243
FOXP3 PE-cy7 (FJK-16s)	Thermo Fisher	Cat#25-5773-82; RRID: AB_891552
Tbet PE (4B10)	Biolegend	Cat#644810; RRID: AB_2200542
CD44 PE-CY7 (IM7)	Biolegend	Cat#103030; RRID: AB_830787
CD62L PE (MEL-14)	Biolegend	Cat#104408; RRID: AB_313095
Epcam PerCp/Cy5.5 (G8.8)	Biolegend	Cat#118220; RRID: AB_2246499
CD19 FITC (1D3/CD19)	Biolegend	Cat#152404; RRID: AB_2629813
NK1.1 BV605 (PK136)	Biolegend	Cat#108753
CD11C BV605 (N418)	Biolegend	Cat#117334
TER119 BV605 (TER-119)	Biolegend	Cat#116239; RRID: AB_2562447
F4/80 BV605 (BM8)	Biolegend	Cat#123133; RRID: AB_2562305
CD3ε BV605 (145-2C11)	Biolegend	Cat#100351; RRID: AB_2565842
Ly6G BV605 (1A8)	Biolegend	Cat#127639; RRID: AB_2565880
B220 PE-cy7 (RA3-6B2)	Biolegend	Cat#103222; RRID: AB_313005
IgA PE (mA-6E1)	Thermo Fisher	Cat#12-4204-81; RRID: AB_465916
IgA AF647 goat polyclonal	Southern Biotech	Cat#1040-31; RRID: AB_2794377
Anti-mouse IFNγ (XMG1.2)	BioXCell	Cat#BE0055; RRID: AB_1107694
Rat IgG1 isotype anti-HRP (HRPN)	BioXCell	Cat#BE0088; RRID: AB_1107775
Anti-mouse IL-17a (17F3)	BioXCell	Cat#BE0173; RRID: AB_10950102
Mouse IgG1 isotype (MOPC-21)	BioXCell	Cat#BE0083; RRID: AB_1107784
Anti-mouse TNFa (TN3-19.12)	BioXCell	Cat#BE0244; RRID: AB_2687725
Polyclonal hamster IgG	BioXCell	Cat#BE0091; RRID: AB_1107773
Anti-GATA4 (G4)	SantaCruz	Cat#sc-25310; RRID: AB_627667
Bacterial and virus strains		
Citrobacter rodentium DBS120 *pler-lux*	Alexander Chervonsky	Pickard et al.[56]

(*Continued on next page*)

Continued

REAGENT or RESOURCE	SOURCE	IDENTIFIER
Citrobacter rodentium DBS100	Gabriel Nuñez	Atarashi et al.[14]
Citrobacter rodentium DBS100 ΔEAE	Gabriel Nuñez	Atarashi et al.[14]
Mouse segmented filamentous bacteria	Kenya Honda	Atarashi et al.[14]
Rat segmented filamentous bacteria	Kenya Honda	Atarashi et al.[14]
Biological samples		
Fetal Bovine Serum	Biowest	Cat#S01520; Lot#A11504E
Normal Goat Serum	JacksonImmunoResearch	Cat#005-000-121
Chemicals, peptides, and recombinant proteins		
EDTA, 0.5M, pH8.0	Corning	Cat#46-034-CI
1M MgCl2	Thermo Fisher	Cat#AM9530G
Cytiva Percoll™ Centrifugation Media	GE Healthcare	Cat#45-001-747
RNAprotect Tissue Reagent	Qiagen	Cat#76106
2-Mercaptoethanol (BME)	Sigma-Aldrich	Cat#M7154
Phorbol Myristate Acetate	Sigma-Aldrich	Cat#P1585
Ionomycin Calcium Salt from Streptomyces conglobatus	Sigma-Aldrich	Cat#10634
BD GolgiStop Protein Transport Inhibitor	BD	Cat#554724
Ethanol 200 Proof	Decon Labs Inc	Cat#DSP-MD 43
Inhibitex Buffer	Qiagen	Cat#19593
Nuclease-free Water	Ambion	Cat#AM9932
Carnoy Solution	Ricca Chemical	Cat#R18510004C
10% Formalin Solution	Thermo Fisher	Cat#SF98-4
RPMI 1640 with L-Glutamine	Corning	Cat#MT-10043CV
Collagenase from *Clostridium histolyticum*	Sigma-Aldrich	Cat#C2139-500MG
1M TRIS-HCL pH 7.5	Thermo Fisher	Cat#15567027
10% SDS solution	Thermo Fisher	Cat#15553027
Sodium chloride	Sigma-Aldrich	Cat#S9888
All-*trans*-Retinoic acid	Sigma-Aldrich	Cat#R2625
Critical commercial assays		
SytoBC	Thermo Fisher	Cat#S34855
LIVE/DEAD® Fixable Aqua Dead Cell Stain Kit	Thermo Fisher	Cat#L34966
Zombie NIR™ Fixable Viability Kit	Biolegend	Cat#423106
BD Cytofix/Cytoperm Plus Fixation/Permeabilization Solution Kit	BD	Cat#554714
eBioscience™ Foxp3/Transcription Factor Staining Buffer Set	Thermo Fisher	Cat#00-5523-00
QIAamp Fast DNA Stool Mini Kit	Qiagen	Cat#51604
RNeasy Plus Mini Kit	Qiagen	Cat#74136
RNeasy Micro Kit	Qiagen	Cat#74004
GoScript Reverse Transcriptase Kit	Promega	Cat#A5001
SYBR Advantage qPCR Premix	Clontech	Cat#639676
ProLong™ Diamond Antifade Mountant with DAPI	Thermo Fisher	Cat#P36962
Pierce™ Protein L Magnetic Beads	Thermo Fisher	Cat#88850
Pierce™ IgG Elution Buffer, pH 2.0	Thermo Fisher	Cat#21028
1.0 M Tris HCl pH 8.5	VWR	Cat#76236-402
ALDEFLUOR™ Kit	Stemcell technologies	Cat#01700
IgA mouse ELISA	Thermo Fisher	Cat#88-50450-86
QX200 droplet digital PCR system	BioRad	Cat#1864001
QX200 ddPCR EvaGreen Supermix	BioRad	Cat#1864034

(*Continued on next page*)

Continued

REAGENT or RESOURCE	SOURCE	IDENTIFIER
5Prime Hotstart Mastermix	QuantaBio	Cat#2200410
Evagreen	Biotium	Cat#31000
KAPA library quantification kit	Roche	Cat#07960140001
AmpureXP beads	Beckman Coulter	Cat#A63880
Deposited data		
RNA sequencing data	This paper	GEO: GSE205743
16S rRNA sequencing data	This paper	BioProject: PRJNA797871
Experimental models: Organisms/strains		
Mouse: GATA4fl/fl villin-cre	Polly Matzinger laboratory	Shulzhenko et al.[23]
Mouse: germ-free GATA4fl/fl villin-cre	This study	N/A
Mouse: B6 GATA4fl/fl villin-cre	This study	N/A
Mouse: C57BL/6J	Jackson laboratory	JAX: 000,664
Mouse: B6-Tg(Tcra, Tcrb)2Litt/J	Jackson laboratory	JAX: 027,230
Mouse: B6.SJL-*Ptprc*^{a} *Pepc*^{b}/BoyJ	Jackson laboratory	JAX: 002,014
Mouse: B.6129S7-Rag1^{tm1mom}/J	Jackson laboratory	JAX: 002,216
Mouse: CD-1 IGS	Charles River	Crl: CD1
Mouse: B6 Jh−/−	Albert Bendelac laboratory	N/A
Mouse: B6 IgA−/−	Albert Bendelac laboratory	N/A
Oligonucleotides		
GAPDH Forward 5′-AGGTCGGTGTGAACGGATTTG-3′	Abadie et al.[45]	N/A
GAPDH Reverse 5′-TGTAGACCATGTAGTTGAGGTCA-3′	Abadie et al.[45]	N/A
IFNγ Forward 5′-GGATGCATTCATGAGTATTGC-3′	Abadie et al.[45]	N/A
IFNγ Reverse 5′-CCTTTTCCGCTTCCTGAGG -3′	Abadie et al.[45]	N/A
IL-17a Forward 5′-TTTAACTCCCTTGGCGCAAAA-3′	This study	N/A
IL-17a Reverse 5′-CTTTCCCTCCGCATTGACAC-3′	This study	N/A
TNFa Forward 5′-TGGGAGTAGACAAGGTACAACCC-3′	This study	N/A
TNFa Reverse 5′-CATCTTCTCAAAATTCGAGTGACAA-3′	This study	N/A
ASL Forward 5′-TCTTCGTTAGCTGGCAACTCACCT-3′	Klose et al.[57]	N/A
ASL Reverse 5′-ATGACCCAGCAGCTAAGCAGATCA-3′	Klose et al.[57]	N/A
Uni 16S 340F 5′-ACTCCTACGGGAGGCAGCAGT-3′	Sano et al.[58]	N/A
Uni 16S 514R 5′-ATTACCGCGGCTGCTGGC-3′	Sano et al.[58]	N/A
SFB 736F 5′-GACGCTGAGGCATGAGAGCAT-3′	Sano et al.[58]	N/A
SFB 844R 5′-GACGGCACGGATTGTTATTCA-3′	Sano et al.[58]	N/A
ASF457F 5’ -TGCAAGAATGAAACTCAAAGGAAT-3′	Deloris Alexander et al.[59]	N/A
ASF457R 5′- TAAGGTTCTTCGGTTAGCATCGA-3′	Deloris Alexander et al.[59]	N/A
C. rodentium espBF 5′- ATGCCGCAGATGAGACAGTTG-3′	Sagaidak et al.[60]	N/A
C. rodentium espBR 5′-CGTCAGCAGCCTTTTCAGCTA-3′	Sagaidak et al.[60]	N/A
EUB338 5′-Alexa546-GCTGCCTCCCGTAGGAGT-3′	Amann et al.[61]	N/A
EUB338 5′-Cy3-GCTGCCTCCCGTAGGAGT-3′	Amann et al.[61]	N/A
SFB1008 5′-Alexa488-GCGAGCTTCCCTCATTACAAGG-3′	Sano et al.[58]	N/A
SFB1008 5′-Cy5-GCGAGCTTCCCTCATTACAAGG-3′	Sano et al.[58]	N/A
Uni 16S 519F 5′-CAGCMGCCGCGGTAA-3′	Barlow et al.[50]	N/A
Uni 16S 806R 5′-GGACTACHVGGGTWTCTAAT-3′	Barlow et al.[50]	N/A
Tjp1F 5′-AGGACACCAAAGCATGTGAG-3′	Tsai et al.[62]	N/A
Tjp1R 5′-GGCATTCCTGCTGGTTACA-3′	Tsai et al.[62]	N/A
Tjp2F 5′-ATGGGAGCAGTACACCGTGA-3′	Tsai et al.[62]	N/A
Tjp2R 5′-TGACCACCCTGTCATTTTCTTG-3′	Tsai et al.[62]	N/A
Tjp3F 5′-TCGGCATAGCTGTCTCTGGA-3′	Tsai et al.[62]	N/A
Tjp3R 5′-GTTGGCTGTTTTGGTGCAGG-3′	Tsai et al.[62]	N/A

(*Continued on next page*)

Continued

REAGENT or RESOURCE	SOURCE	IDENTIFIER
OclnF 5′-GCTGTGATGTGTGTGAGCTG-3′	Tsai et al.[62]	N/A
OclnR 5′-GACGGTCTACCTGGAGGAAC-3′	Tsai et al.[62]	N/A
Cldn2F 5′-GGCTGTTAGGCACATCCAT-3′	Tsai et al.[62]	N/A
Cldn2R 5′-TGGCACCAACATAGGAACTC-3′	Tsai et al.[62]	N/A
Jam1F 5′-ACCCTCCCTCCTTTCCTTAC-3′	Tsai et al.[62]	N/A
Jam1R 5′-CTAGGACTCTTGCCCAATCC-3′	Tsai et al.[62]	N/A
Cdh1F 5′-TCCTTGTTCGGCTATGTGTC-3′	Tsai et al.[62]	N/A
Cdh1R 5′-GGCATGCACCTAAGAATCAG-3′	Tsai et al.[62]	N/A
Pigr F 5′-GTAACCGAGGCCTGTCCTTC-3′	This study	N/A
Pigr R 5′-GTAGACGTGGGTGTCACTCG-3′	This study	N/A
Software and algorithms		
QIIME2: 2020.2.0	Bolyen et al.[63]	N/A
Silva 132 SSURef NR99	Quast et al.[64]	N/A
Python 3.7.6	https://www.python.org/	N/A
Scipy 1.4.1	https://www.scipy.org/	N/A
Statsmodels 0.10.1	https://www.statsmodels.org/stable/index.html	N/A
Numpy 1.18.1	https://numpy.org/	N/A
Pandas 1.0.3	https://pandas.pydata.org/	N/A
GraphPad Prism 8	https://www.graphpad.com	N/A
FlowJo 10	https://www.flowjo.com	N/A
Other		
Bead ruptor elite bead mill homogenizer	Omni International	Cat#19-040E
Tissue-Tearor	Biospec Products	Cat#985370-XL
Glass Beads	Biospec Products	Cat#11079101
LightCycler® 480 System	Roche	N/A
LSRFortessa™ X-20 Flow Cytometer	BD	N/A
Cytek® Aurora	Cytek	N/A
CRi Pannoramic SCAN 40x Whole Slide Scanner	3DHistech	N/A
EasyEights™ EasySep™ Magnet	Stemcell technologies	Cat#18103
CFX96 Touch RT-PCR detection system	BioRad	Cat#1855196
Mouse RNAseq analysis	This paper	http://doi.org/10.5281/zenodo.7255834.
Human RNAseq analysis	This paper	https://doi.org/10.5281/zenodo.7272314

RESOURCE AVAILABILITY

Lead contact

Further information and requests for resources and reagents should be directed to and will be fulfilled by the lead contact, Bana Jabri (bjabri@bsd.uchicago.edu).

Materials availability

All reagents generated or used in this study are available on request from the lead contact with a completed Materials Transfer Agreement. Information on reagents used in this study is available in the key resources table.

Data and code availability

All the data supporting the findings of the article are available within the main text or supplementary information. The published article includes datasets generated during this study. Original RNA-seq data has been deposited in GEO: GSE205743. Original 16S rRNA sequencing datasets analyzed in this study are available at the NCBI BioProject: PRJNA797871. Any additional information required to reanalyze the data reported in this paper is available from the lead contact upon request. Original code for analyzing these datasets have been deposited in Zenodo and is publicly available. DOIs are listed in the key resources table.

EXPERIMENTAL MODEL AND SUBJECT DETAILS

Mice

7-12 week old mice were used for experiments, co-housed in specific pathogen-free conditions, and kept *Helicobacter hepaticus*, murine norovirus free at the University of Chicago. Some mice were also housed in gnotobiotic isolators and routinely checked for sterility by culture and 16S PCR or kept SFB monocolonized at the University of Chicago Gnotobiotic Research Animal Facility. GATA4fl/fl villin-cre SPF mice were previously generated in the CD1 background and obtained from the Matzinger laboratory.[23] This line was rederived GF for this study and backcrossed for 10 generations to C57BL/6J background for T cell transfers. C57BL/6J, B6-Tg(Tcra, Tcrb)2Litt/J SFB TCRtg, B6.SJL-*Ptprc*^{a} *Pepc*^{b}/BoyJ, B.6129S7-Rag1^{tm1mom}/J were obtained from the Jackson Laboratory. CD-1 IGS mice were obtained from Charles River Laboratories. B cell deficient mice deficient for IgH J segment locus (JH), recreating the previously described model,[24] were generated at University of Chicago and obtained from Dr. Bendelac at the University of Chicago on a C57BL/6 background using Cas9 with the protospacers GCTACTGGTACTTCGATGTC and GCCATTCTTACCTGAG GAGA. IgA deficient mice where the Sα (IgA switch region) and C1α (first exon) were deleted, as previously described,[55] were generated at University of Chicago and obtained from Dr. Bendelac on a C57BL/6 background using Cas9 with the protospacers AAGCGGCCACAACGTGGAGG and TCAAGTGACCCAGTGATAAT. Jh and IgA deficient mice were rederived GF at Taconic Biosciences. Littermate controls of GATA4, Jh, and IgA were used for all experiments in this study. Mice were fed a standard chow diet, vitamin A control diet (Harlan TD.91280), or vitamin A deficient diet (Harlan TD. 86143). Animal husbandry and experimental procedures were performed in accordance with Public Health Service policy and approved by the University of Chicago Institutional Animal Care and Use Committees.

Patients

A duodenal biopsy was obtained from 166 individuals undergoing upper gastrointestinal endoscopy at the University of Chicago and at Mayo Clinic as previously reported.[45] There were 64 control patients, 56 untreated patients with active celiac disease, and 46 patients treated with a gluten free diet. All control patients underwent endoscopies for issues unrelated to celiac disease and had normal intestinal histology, no family history of celiac disease, and no significant levels of anti-TG2 antibodies in the serum. Patients with active celiac disease contained positive anti-TG2 antibodies and small intestinal enteropathies with increased IEL infiltration, crypt hyperplasia, and villous atrophy according to the accepted diagnostic guidelines.[65] The subjects signed an informed consent as provided by the Institutional Review Board of each institution (IRB-12623B for the University of Chicago, and IRB-1491-03 for the Mayo Clinic). DNA and RNA were isolated from each biopsy as described previously[45] using the AllPrep DNA/RNA mini kit (Qiagen).

C. rodentium infections

C. rodentium strains DBS100, DBS120 *pler-lux*, or DBS100 ΔEAE were grown at 37°C in Luria broth under agitation.[14,56] The cultures were diluted 100X and grew to log phase until the OD^{600nm} reached 0.75. For gavage, 200 μL of bacteria were used, which gave a dose of 2.5×10^{9} CFU/mouse. Mice were separated into cages based on genotype for infections, and male mice were used for survival studies. DBS100 or DBS100 ΔEAE strains were given to GF mice and DBS120 *pler-lux* was given to SPF mice. The DBS120 strain has a genomic kanamycin resistance cassette inserted through Tn5. To determine CFUs of DBS120, 2 fecal pellets/mouse were resuspended in 1 mL of PBS and plated on MacConkey agar containing 50 μg/mL of kanamycin. The CFU/mg feces concentration was determined as: (#CFU counted*Dilution factor/(vol plated in ml))/mg feces. To determine the amount of bacterial translocation, the MLN, liver, and spleen were aseptically dissected, weighed, and homogenized with the Tissue-Tearor rotor (BioSpec) in 500 μL of PBS. Then 200 μL of homogenate was plated on MacConkey agar containing 50 μg/ml of kanamycin. For infections of SFB free mice, JAX colonized WT and GATA4$^{\Delta IEC}$ mice were colonized with SFB as described below at approximately 6 weeks of age and infected with *C. rodentium* two weeks later. For cytokine neutralizations, WT and GATA4$^{\Delta IEC}$ mice were treated i.p with 250 μg of either isotype control or αTNF, αIL-17a, or αIFNγ neutralizing antibodies on days 3, 5, 7, and 9 after infection.

Microbial transfers

To colonize mice with SFB[56] or rat SFB,[14] 3–4 fresh fecal pellets from SFB monocolonized mice were homogenized in 1 mL of PBS, vortexed for 3 min, and spun at 300 g to remove large debris. Then 200 μL of the homogenate were gavaged to recipient mice. When possible, SFB donor pellets were taken from monocolonized Jh or IgA deficient mice, which harbor 10-fold higher levels of SFB. To colonize mice with SFB-free microbiota, C57BL6 mice from Jackson Labs, which lack SFB in the microbiota, were used as donor mice. Small intestinal and cecal contents were pooled for one donor mouse homogenized in PBS, and gavaged to recipient mice with or without SFB supplemented. For WT and GATA4$^{\Delta IEC}$ microbiota transfer to GF WT and GATA4$^{\Delta IEC}$ hosts, jejunal content was pooled from two donor SPF GATA4$^{\Delta IEC}$ mice or littermate WT mice. Colonization of ASF strains (Taconic) was performed as described previously[66] and gavaged to recipient WT and GATA4$^{\Delta IEC}$ mice. For all microbial transfers, mice were colonized at 4 weeks of age and analyzed at 8 weeks.

Vitamin A deficient diet

GF C57BL6 mice were placed on control (Harlan TD.91280) or vitamin A deficient (Harlan TD. 86143) diets from 4 to 8 weeks of age. At 8 weeks, mice were monocolonized with SFB for one week as described above, and the amount of SFB in jejunal mucosal scrapings was quantified by qPCR.

SFB TCRtg adoptive transfer

Naive SFB TCRtg Vβ8 CD4$^+$ T cells were isolated from LNs and spleen of congenically marked CD45.1 Vβ8$^{+/-}$ female mice using the naive CD4 T cell isolation kit (Miltenyi), and 2x10^5 cells/100 μL mouse were injected retroorbitally into CD45.2 WT and GATA4$^{\Delta IEC}$. Three days after transfer, the mice were euthanized to assess T cell priming and activation in the jejunal and ileal draining MLN as described previously (Esterházy et al., 2019). To assess T cell expansion in the LP of the jejunum nine days after transfer, 50,000 cells were injected/mouse.

METHOD DETAILS

Isolation of intestinal epithelial cells (IEC), intraepithelial lymphocytes (IEL), and lamina propria (LP) cells

The segments of the intestine were excised as follows to isolate cells for flow cytometry: duodenum was taken 12 cm from the stomach, jejunum 12 cm from the middle, and ileum 12 cm from the cecum. Any leftover segments were discarded. The entire colon was taken after the cecum to the rectum. To isolate IEL and IECs, Peyer's patches were first removed from the small intestine, and then the segments were opened longitudinally and washed briefly in PBS (PBS). Epithelial cells, including IELs and LP cells, were isolated as previously described[67] using EDTA containing calcium-free media and collagenase VIII (Sigma-Aldrich, C2139), respectively. The IEL and LP compartments were then subjected to a 40% percoll density gradient centrifugation step to remove dead cells and debris as previously described.[45] The IEL and LP cells were then counted on a hemocytometer.

Cytokine stimulation

Up to 2x10^6 cells were collected and resuspended in RPMI 1640 media with 10% fetal bovine serum (FBS) and cultured in 48-well plates in the presence of 750 ng/mL of ionomycin, 50 ng/mL of Phorbol 12-myristate 13-acetate (Sigma-Aldrich), and golgi-stop (BD). The cells were incubated for 2 h at 37C with 5% CO_2. After stimulation, the reaction was quenched with ice-cold FACS buffer, and the cells were subsequently stained with antibodies for flow cytometry.

Flow cytometry

The cells were first stained with FC block (CD16/32) to block nonspecific binding and then were stained with dead dye to exclude dead cells (Aqua, ThermoFisher or Zombie NIR, Biolegend) for 15 min at 4°C, followed by staining with cell surface markers for 20 min at 4°C. For intracellular cytokine staining, the BD cytofix/cytoperm kit was used, and cells were incubated with the antibodies for 40 min at 4°C. For intracellular transcription factors, the Foxp3 eBioscience kit was used according to the manufacturer's instructions. The antibodies used are indicated in key resources table. For ALDH staining of IECs, the ALDEFLUOR kit was used (StemCell Technologies), following the manufacturer's protocol. All cells were gated FSC, SSC, singlets, and live cells. IECs were gated CD45$^-$ EpCAM$^+$. 100,000 IECs from the jejunum or ileum were sorted with Aria Fusion (BD Biosciences) into RLT buffer (Qiagen) with β-mercaptoethanol for downstream sequencing analysis. IgA plasma cells were gated as described previously,[26] i.e. EpCAM$^-$, CD45$^+$/dim, lineage negative (Ter119, F4/80, CD3, Ly6G, NK1.1, CD19), IgA$^+$, B220$^-$. CD8αβ IELs were gated TCRβ$^+$, CD4$^-$, CD8α+, CD8β$^+$. CD4$^+$ LP T cells were gated TCRβ$^+$, CD4$^+$, CD8α$^-$. The following antibodies and clones were purchased from Biolegend: CD45 Pacific Blue (30-F11), CD4 BV785 (GK1.5), CD4 BV605 (GK1.5), IL10 PE-Cy7 (JES5-16E3), CD45.1 Pacific Blue (A20), Tbet PE (4B10), CD44 PE-Cy7 (IM7), CD62L PE (MEL-14), Epcam PerCP-Cy5.5 (G8.8), CD19 FITC (1D3/CD19), NK1.1 BV605 (PK136), CD11C BV605 (N418), TER119 BV605 (TER-119), F4/80 BV605 (BM8), CD3ε BV605 (145-2C11), Ly6G BV605 (1A8), B220 PE-Cy7 (RA3-6B2). The following antibodies and clones were purchased from BD: CD8β BUV395 (H35–17.2), CD8α PerCP-Cy5.5 (53-6.7), NK1.1 PE-CF594 (PK136), TCRβ BUV737 (H57-597), TCRβ BV711 (H57-597), CD3ε BUV737 (145-2C11), IFN-g APC (XMG1.2), TNF BB700 (MP6-XT22), CD45.2 BUV395 (104), vβ14 TCR FITC (14-2), RORγt BV786 (Q31-37). The following antibodies and clones were purchased from Thermo Fisher: TCRgd FITC (eBioGL3), IL17a PE (ebio17B7), FOXP3 eFluor450 (FJK-16s), FOXP3 FITC (FJK-16s), FOXP3 PE-Cy7 (FJK-16s), IgA PE (mA-6E1). The cells were run on the LSRFortessa X-20 Flow Cytometer (BD Biosciences) or the Cytek Aurora and data were analyzed using FlowJo software (Treestar).

DNA isolation

For mucosal scrapings for DNA isolation, 5 cm of tissue proximal to the middle of the intestine was taken for the jejunum, and 5 cm from the ileocecal valve was taken for the ileum. The entire colon was used for mucosal scrapings. The tissue was excised, opened longitudinally, scraped with a glass slide, transferred to 2 mL screw cap tube containing 0.1 mm glass beads (Bio-spec), and snap frozen on dry ice. For luminal content, 50-100 mg of content was taken from as close to the middle of the jejunum as possible and from the last 5–7 cm of the ileum. Homogenization was performed after adding 1 mL of inhibitex buffer (Qiagen) using the Bead Ruptor Elite bead mill homogenizer (Omni, 19040E) on speed 6 for 3 min. DNA was then extracted using the QIAmp Fast DNA stool mini kit (Qiagen) following the manufacturer's protocol with the optional high temp (95°C) lysis step. DNA concentration was determined using the nanodrop UV spectrophotometer (ThermoFisher).

RNA isolation

For eventual RNA purification, 1 cm of tissue was excised from the beginning of the duodenum, the middle of the jejunum, the end of the ileum, and the center of the colon and preserved in RNAprotect (Qiagen) overnight at 4°C and then transferred to −80°C for long-term storage. The tissue was transferred to 600 μL of RLT buffer containing β-mercaptoethanol (Qiagen) and homogenized for 30 s

with a hand held rotor (Tissue-Tearor, BioSpec). RNA was purified using RNAeasy plus mini kit (Qiagen) following the manufacturer's protocol with the optional on column DNase digest (Qiagen).

qPCR

RNA was first reverse-transcribed to cDNA using GoScript Reverse Transcriptase kit (Promega) following the manufacturers protocol. For qPCR, 10 ng of cDNA or 20 ng of DNA from mucosal scrapings and content was used. TB green Advantage qPCR Premix (Takara) was used, and the target gene was quantified and normalized to the housekeeping gene as described previously[45] using $1000*2^{-(Ct\ target-\ Ct\ housekeeping)}$ formula. For host gene expression, the target gene was normalized to GAPDH. For bacterial load, the target gene was normalized to either host DNA as described previously[58] with primers specific for host argininosuccinate lyase (ASL) gene or universal 16S primers. The qPCR was performed on the LightCycler 480 System (Roche). The primer pairs and DNA sequences are included in key resources table.

Histology

The tissue was collected in the same manner as for RNA, placed in cassettes and fixed in 10% formalin for H&E staining or Carnoy solution (ThermoFisher) for fluorescent *in situ* hybridization (FISH) staining overnight at room temperature. Cassettes were transferred to 70% ethanol for formalin or 100% ethanol after Carnoy fixation to wash out the fixative. The tissue was embedded in paraffin, and slides were cut at 5 μm thickness. The H&E staining was performed by the Human Tissue Resource Center at the University of Chicago. For FISH staining, the paraffin was first removed by running the slides through four 3-min incubations in xylene and four 3-min incubations in 100% ethanol. The slides were then moved to a polypropylene slide container and filled with hybridization solution containing the diluted 16S probe (0.9M NaCl, 20mM Tris-HCL pH 7.5, 0.1% SDS with 0.2 ng of probe specific for SFB 16S or universal 16S).[68] The 16S probes used are included in key resources table. The slides were incubated overnight at 50°C in the dark. The slides were washed three times with the hybridization buffer, briefly rinsed in H_20, and then mounted with Prolong diamond antifade with DAPI (ThermoFisher). The slides were scanned with the CRi Pannoramic SCAN 40x Whole Slide Scanner at the University of Chicago Integrated Light Microscopy core.

Transmission electron microscopy

2 cm of jejunum tissue was open longitudinally and fixed in 2% glutaraldehyde, 4% paraformaldehyde, in 0.1M sodium cacodylate buffer for 2 h. The fixative was then replaced with 1% osmium tetroxide in 0.1M sodium cacodylate buffer for 60 min. The tissue was subsequently washed 2X for 5 min with sodium cacodylate buffer and finally with maleate buffer (pH 5.1). 1% uranyl acetate in maleate buffer was added for 60 min, and the tissue was washed again with maleate buffer 3X for 5 min. The tissue was next dehydrated by running through 25%, 50%, 70%, 95% ethanol for 2 × 5 min each and ending on 100% ethanol for 3 × 15 min. Finally 100% propylene oxide was added for 3 × 15 min 2:1 propylene oxide spurr resin was added 2 × 30 min, and 1:1 propylene oxide spurr resin was added 2 × 30 min and overnight, next day 100% spur resin was added 6 × 60 min. The polymerized spur with embedded tissue was put into a 60C oven for 1-2 days 90 nm sections were cut by Leica EM UC6, stained with uranyl acetate and lead citrate. Images were examined under 300 kV at FEI Tecnai F30 Gatan CCD digital micrograph.

ELISA

To quantify luminal IgA levels, content was collected from the jejunum and ileum and weighed in 2-mL bead beating tubes containing 0.1 mm glass beads. After adding 1 mL of 1X cell lysis buffer with protease inhibitors (Cell Signaling Technologies), the content was homogenized on a vortex for 5 min. The debris were pelleted at 13,000 rpm for 10 min, and the supernatant was collected for ELISA. For tissue explants, 1 cm of tissue was excised and opened longitudinally, washed in PBS, and placed in complete RPMI at 37°C for 24 h. The culture supernatant was collected and used for ELISA. The supernatant was diluted in 1X assay diluent A (ThermoFisher), and the dilution in the middle of the standard curve was used to quantify IgA levels. IgA mouse uncoated ELISA kit (ThermoFisher) was used following the manufacturer's protocol, and absorbance was read at 450 nm. The amounts of IgA were back calculated to the original sample and normalized relative to the weight of the content or to ml of culture supernatant.

Luminal IgA isolation and *in vivo* treatment

To isolate luminal polyclonal sIgA from the intestine, luminal content was pooled from the small intestine, large intestine, and cecum from SFB+ 8–12 week old WT CD1 mice (Charles river). Content was transferred to falcons containing 1X Tris-Buffered Saline, 0.1% Tween 20 (TBST) buffer with proteinase inhibitor (Roche). Falcons were then vortexed for 5 min on max speed and centrifuged for 10 min at 5000 rpm. The supernatant was collected and spun again two times to further remove bacteria and debris. Pierce Protein L Magnetic Beads (Thermo Scientific) were added and incubated for 1 h at room temperature while shaking. After 1 h, beads selectively bound to IgA through kappa light chain were separated from the supernatant with EasySep magnetic stand (StemCell technologies). Supernatant was discarded and beads washed 3 times. IgA was separated from the beads with Pierce IgG Elution Buffer pH 2.0 (ThermoFisher). Elution buffer was incubated with the beads for 10 min at room temperature on a shaker. Tris-HCl 1M pH 8.5 was added to neutralize the solution. IgA protein concentration was measured using NanoDrop. The isolated IgA preparation was then filtered with 0.22 μm sterile syringe filter unit. The IgA preparation was kept up to one week at 4°C. When IgA were administered to the mice by gavage, the isolated IgA preparation was further concentrated with Amicon Ultra-4 Centrifugal Filter Units (MilliporeSigma) until 250–350 μg/0.1 mL final concentration was achieved. To optimize the treatment protocol to restore luminal

IgA levels *in vivo* to GATA4$^{\Delta IEC}$ mice, we first treated RAG−/− mice with 250 μg of the IgA preparation. After 1 h, we assessed the frequency of IgA$^+$ bacteria in small intestinal contents by flow cytometry as described below, and noted 10–20% of bacteria were IgA$^+$ after gavage. The bacterial coating was transient due to intestinal flow and undetectable after 2 h. Therefore, continuous IgA gavages were necessary to sustain luminal IgA and bacterial coating in the small intestine. To administer the IgA preparation and analyze SFB colonization, GF, WT and GATA4$^{\Delta IEC}$ mice were gavaged with 100 μL of IgA or PBS. After 1 h, the mice were colonized with SFB and gavaged again with IgA or PBS. Three more gavages were performed at 2-h intervals. The mice were euthanized 24 h after the gavage of SFB, and the regionalization of SFB load was assessed in jejunal and ileal mucosal scrapings by qPCR.

In-vivo retinoic acid treatment

All-*trans*-retinoic acid (Sigma) was resuspended in DMSO at a concentration of 20 mg/ml, diluted in corn oil, and administered to mice at a dose of 300 μg i.p every other day for 14 days.

Bacterial staining with luminal IgA

Luminal content was taken from WT, GATA4$^{\Delta IEC}$, or RAG−/− mice and resuspended in 1X PBS with protease inhibitors at a concentration of 0.1 mg/μl, vortexed for 5 min, and spun at 8000 rpm for 5 min. Three fecal pellets from RAG−/− mice were homogenized and pelleted. The bacterial pellet was resuspended in 50 μL PBS and combined with 50 μL of luminal supernatant containing IgA. The IgA was incubated with the bacteria for 1 h at 4°C. The bacteria were then washed, pelleted, and stained with SYTO BC (ThermoFisher) diluted 1:5000 and anti-IgA APC (Southern Biotech) diluted 1:200 for 30 min. Bacteria were gated on FSC, SSC, SYTOBC$^+$, and IgA$^+$.

Microbial 16S sequencing: Library generation and initial data processing

Extracted DNA was amplified, barcoded and sequenced as described previously.[50,69,70] Briefly, amplification of the variable 4 (V4: 519F-806R) region of the 16S rRNA gene was performed with total DNA input (determined by NanoDrop) limited to 400 ng to prevent inefficient amplification. Amplification was stopped in late exponential phase to minimize chimera formation. Amplified libraries were combined at equimolar concentrations and sequenced on an Illumina MiSeq (2x300 bp). Fastq files were processed with QIIME 2 2020.2 [62] using dada2 for amplicon sequence variant (ASV) determination and the Silva 132 99% OTUs reference database for taxonomy assignment. Rarefaction to the lowest read depth present in all samples (48,305 reads) was performed to decrease biases from varying sequencing depth between samples.[71]

Microbial 16S sequencing: Absolute abundances

The total microbial load (bacteria and archaea) of each sample and the absolute abundance of each taxon in individual samples was determined as described previously.[50,69] Briefly, the Bio-Rad QX200 droplet dPCR system (Bio-Rad Laboratories) with primers targeting the V4 (519F-806R) region was utilized to measure the number of 16S rRNA gene copies per sample. The final concentration of 16S rRNA gene copies in each sample was normalized to the extracted sample total DNA measurement from NanoDrop. Total DNA levels provide a good proxy for tissue mass in biopsy samples. The input-DNA-normalized total microbial load was multiplied by each ASV's relative abundance to determine the absolute abundance of each ASV.

Microbial 16S sequencing data analysis: Poisson quality filtering

Poisson quality filtering of low abundance taxa was performed as previously described.[72] Briefly, the relative abundance limit of detection (LOD) was determined for each sample. Relative abundance LOD is a function of two Poisson sampling steps: one based on the number of 16S molecules input into the library amplification reaction, and the other by the number of sequencing reads generated from the amplicon library. In each case, the relative abundance LOD was set at the point where 95% confidence of detection was observed and then the minimum of the two described LODs was used. For each sample, the relative abundance of each ASV detected below the LOD was set to zero.

Microbial 16S sequencing data analysis: Statistical analysis

Group comparisons were analyzed using the non-parametric Kruskal-Wallis rank sums tests with Benjamini–Hochberg multiple hypothesis testing correction using *SciPy.stats Kruskal* function and *statsmodels.stats.multitest multipletests* function with the *fdr_bh* option.

RNA-seq of purified IECs from mice

To perform RNA-seq on IECs, 100,000 EPCAM+ CD45$^-$cells were cell sorted from the jejunum and ileum of WT and GATA4$^{\Delta IEC}$ mice. Three independent cell sorting experiments were performed and the libraries and sequencing were done on the same batch with 8 mice per group. The SMART-Seq v4 Ultra Low Input RNA Kit (TaKaRa) was used to generated amplified cDNA, using either 7500 pg of RNA input. The cDNA was generated and purified according to the manufacturer's specifications. cDNA was amplified 12 cycles based on empiric testing. The Nextera XT DNA Library Preparation Kit (Illumina) was used to generate the RNA-seq libraries, with an input of 125 pg cDNA, according to the manufacturer's specifications. Subsequently, the libraries were multiplexed and sequenced at a depth of 20 million reads per sample (50 bp SR) on a HiSeq4000.

Tissue RNA-seq

Whole tissue duodenal biopsies stored at −80C were thawed on ice and transferred to Starstedt tubes containing 350uL RLT Plus supplemented with 1% 2-mercaptoethanol and equal quantities of 1.0 and 0.5 mm zirconium oxide beads (Next Advance). Biopsies were bead beat 3 times for 1 min at a setting of 9 on a Bullet Blender 24, with 1 min of cooling on ice between each beating. Lysates were processed using the AllPrep DNA/RNA/miRNA Universal Kit (Qiagen). 500 ng of purified RNA was used as input in the TruSeq Stranded mRNA Library Prep kit (Illumina) to generate sample libraries according to manufacturer's specifications. Libraries were multiplexed and sequenced at a depth of 20 million reads per sample (50 bp SR) on a HiSeq4000.

Mouse RNA-seq data processing to obtain raw counts

Mouse RNA-seq raw data were processed using a standard workflow based on the GENPIPES framework.[73] Specifically, the "string-tie" type "rnaseq" pipeline was used. Reads were first trimmed using Trimmomatic software.[74] Trimmed reads were aligned to the Mus_musculus.GRCm38 mouse reference genome using the STAR aligner[75] following a two-pass mapping protocol. Alignments were then sorted and filtered for duplicates using Picard(sort, markduplicates) ("Picard Toolkit" Broad Institute http://broadinstitute.github.io/picard/; Broad Institute). Gene-level read counts for downstream processing were calculated from spliced alignments using HTseq count.[76]

Mouse RNA-seq data analysis: Quality control filtering and normalization

All statistical analyses of the mouse RNA-seq data were performed using R (v.4.0.3). From the raw count matrices, genes expressed (*i.e.*, having at least two counts) in fewer than two samples were removed. The resulting matrices will be referred to as the count matrices. Counts were normalized by applying the variance stabilizing transformation (i.e. *vst(),* default parameters) from the DESeq2 R package (v.1.30.1).[77] Batch effects were removed using the *removeBatchEffect()* function (batch = "sort_batch") from the limma R package (v.3.46.0).[78]

Mouse RNA-seq data analysis: Differential expression and gene set enrichment

Comparisons of gene expression between sample groups were made using DESeq2 to fit a negative binomial generalized linear model with a group variable. Wald statistics were used to determine the significance of the group coefficient, i.e., the log2-fold change (LFC) in expression between groups. We used the Benjamini-Hochberg method for controlling the false discovery rate (FDR). The *p* values reported are FDR adjusted. Genes with an adjusted p-value of at most 0.05 were considered differentially expressed (DE) between groups. The LFCs and FDR-adjusted *p* values were given as input to the *fgsea()* function from the fgsea R package (v.1.16.0),[79] which implements a preranked gene set enrichment analysis. The rankings of the genes were based on the FDR-adjusted *p* values. The mouse KEGG pathway database (mmuKegg)[80] and/or the Gene Ontology Biological Processes (GO-BP) database[81,82] were the gene sets used in the enrichment analyses. Enriched pathways (*i.e.*, $p < 0.05$) were collapsed to independent pathways to avoid repetitive terms, using the fgsea *collapsePathways()* function.

Identifying region-specific GATA4-regulated genes

This set of DE genes was determined by grouping together "ileum-like" samples, *i.e.*, WT ileum and GATA$^{\Delta IEC}$ jejunum samples, and comparing them with WT Jejunum samples. Comparisons were performed separately for the tissue and IECs. A threshold of >0.25 for the absolute value of the LFC was used to filter the very high number of DE genes in the tissue RNA-seq data, whereas no LFC threshold was used for the EC data.

Microbiota-dependent and -independent genes

We determined the influence of microbiota on the region-specific GATA4-regulated genes by systematically comparing jejunum tissue samples. For two analyses, we compared genotypes while maintaining a fixed microbiota status; for the third analysis, we jointly analyzed the effects of genotype and microbiota, including an interaction term (we were too underpowered to use only the latter approach). Thus, we identified three groups: (1) DE genes in GATA$^{\Delta IEC}$ SPF, relative to WT SPF, (2) DE genes in GATA$^{\Delta IEC}$ GF, relative to WT GF, and (3) genes with a significant interaction between genotype and microbiota.

(a) Microbiota-dependent genes: Genes that were strongly DE (*i.e.*, $P < 0.01$, $|LFC| > 0.6$) in group 1 but not DE (*i.e.*, $P > 0.2$) in group 2, or vice versa, were deemed microbiota dependent. Furthermore, genes in group 3 that had a strong, significant interaction term (*i.e.*, $P < 0.01$, $|LFC| > 0.9$) were also considered microbiota dependent.
(b) Microbiota-independent genes: Genes that were strongly DE (i.e., $P < 0.01$, $|LFC| > 0.6$) in both groups (with LFC of the same sign) were deemed microbiota independent. Further, genes in group 3 that had a weak or insignificant interaction term (i.e., $P > 0.2$ or $|LFC| < 0.3$) were included.

Both sets of genes, (a) and (b), were then intersected with the previously determined set of region-specific, GATA4-regulated genes, resulting in region-specific, GATA4-regulated genes that were either microbiota dependent or independent.

Mouse RNA-seq data analysis: Data visualization

Principal components plots

The principal components analysis (PCA) was done using the *pca()* function from the PCAtools R package (v.2.2.0.).[83] The top 500 genes selected by highest row variance in the centered (across rows) normalized count matrix were used to calculate the principal

components. For the analysis of the immune genes (Figure 1C), the normalized counts matrix was first intersected with the genes in the immune module. Using the full set of genes to calculate the PCA shows the same patterns but with a larger spread within sample groups.

Heatmaps

Heatmaps were plotted using the *Heatmap()* function from the ComplexHeatmap R (v.2.6.2) package.[84] The z-scored (i.e., across rows) normalized expression values were used to plot the heatmaps.

Annotation of GATA4-targeted genes

A previously published and publicly available table of annotated GATA4 ChIP-Seq peaks[9] was used to annotate GATA4 targets among the DE genes reported.

Generation of immune, IL-17, and IFNγ gene modules

We curated modules of immune genes, IL-17-associated genes, and IFNγ-associated genes. The immune module was created using two curated and publicly available databases: IRIS[7] and ImmPort.[6] These human genes were then converted to mouse homologs. Genes that did not have homologs were discarded. The resulting module consists of 4,279 genes (Table S2.The IL-17 and IFNγ modules consist of known gene pathways from established databases, publications, and experimental data using IFNγ$^{-/-}$, IFNγr$^{-/-}$, IL17$^{-/-}$, IL17r$^{-/-}$, or IFNγ, IL17 treated cell lines or mice. Specifically, the IL-17 module consisted of genes encompassing the following pathways from mmuKEGG: 04,657, 04,659 and msigDB: m6335, m19422, m298, m300, m461, m460, m39560, m8578, m8581, m8579, m8927, m8928, and the following papers.[14,85]

The IFNγ module consisted of genes encompassing the following pathways from msigDB: m22085, m5972, m5970, m4551, m9583, m39363, m161, m6305, m6313, m6696, m6695, m6689, m6688, m6523, m6522, m6513, m6512, m1898, m2913, m8662, m8657, m5913, from the Gene Ontology database: GO:0034341, from the Reactome database: R- 913,531, and the following papers.[86,87]

Human RNA-seq data analysis

Adaptors and low-quality bases were trimmed using Trim Galore (v 0.4.4). Resulting reads were then aligned to the human reference sequence Ensembl GRCh38 release 87 using Kallisto.[88] Next, the derived pseudo counts were normalized into log2 counts per million reads (CPM) using the voom function from the limma package (v3.46.0).[78] To evaluate the transcriptomic changes associated with GATA4 dysregulation in the small intestine and in the context of celiac disease we defined two contrast groups: "GATA4-lo", to reflect loss of regionalization, and "GATA4-hi", as a normal jejunum tissue. Using the normalized expression of GATA4 to rank all control, ACeD and GFD samples, we defined the "GATA4-hi" group as the samples in the top 30% of GATA4 expression (ACeD n = 6, Control n = 18, GFD n = 18). The "GATA4-lo" group was defined by ACeD samples in the bottom 30% of GATA4 expression across only ACeD samples (n = 15). Next, to define a universe set for the differential expression and enrichment analyses, we generated a set of 11,657 homologous genes expressed in the human and mouse cohorts. We then tested transcriptome-wide for significant differences in expression between the GATA4-hi and GATA4-lo groups of samples, using a linear model that accounted for sex, age, batch, and technical covariates, and corrected for multiple testing. Over-enrichment analysis of gene ontologies biological processes were performed using the enrichGO function from the clusterProfiler (v3.0.4).[89] All statistical analyses within the human cohort and the overlaps with the mouse GATA4$^{\Delta IEC}$ dataset were performed using R (v4.0.3).

Using the log2(CPM) expression values, we calculated single sample Gene Set Enrichment scores (ssGSEA) for the retinol pathway, IL17 downstream genes, and the MSigDB hallmark gene sets,[90] using the R Bioconductor Package GSVA.[91] These ssGSEA scores where then used to test association between GATA-hi vs GATA-lo contrasts groups, as well as association with presence or absence of bacteria. Associations were evaluated using a linear model accounting for sex, age and technical covariates.

QUANTIFICATION AND STATISTICAL ANALYSIS

Data were first analyzed for normal distribution using D'Agostino and Pearson omnibus normality tests. Normally distributed data were analyzed with unpaired two-tailed Student's *t* test when comparing two groups, one-way ANOVA followed by Tukey's post-hoc test for multiple comparisons, or two-way ANOVA for comparing two groups against multiple variables. Not normally distributed data were analyzed using two-tailed Mann-Whitney test when comparing two groups, or Kruskal-Wallis with Dunn's multiple comparison test for multiple comparisons. Data in all figures displayed are pooled from a minimum of two-independent experiments and represented as mean ± SEM when possible. Number of samples are reported in each figure legend. The statistical test used and *p* values are indicated in each figure legend and performed with GraphPad Prism 8. *p* values < 0.05 were considered statistically significant. ****p < 0.0001, ***p < 0.001, **p < 0.01, *p < 0.05., or ^{oooo} p < 0.0001, ^{ooo} p < 0.001, ^{oo} p < 0.01, ^{o} p < 0.05.